MAIT Cells Upregulate α4β7 in Response to Acute Simian Immunodeficiency Virus/Simian HIV Infection but Are Resistant to Peripheral Depletion in Pigtail Macaques

Jennifer A. Juno,* Kathleen M. Wragg,* Thakshila Amarasena,* Bronwyn S. Meehan,* Jeffrey Y. W. Mak,[†,‡] Ligong Liu,[†,‡] David P. Fairlie,[†,‡] James McCluskey,* Sidonia B. G. Eckle,*[,1] and Stephen J. Kent*[,§,¶,1]

Mucosal-associated invariant T (MAIT) cells are nonconventional T lymphocytes that recognize bacterial metabolites presented by MR1. Whereas gut bacterial translocation and the loss/dysfunction of peripheral MAIT cells in HIV infection is well described, MAIT cells in nonhuman primate models are poorly characterized. We generated a pigtail macaque (PTM)–specific MR1 tetramer and characterized MAIT cells in serial samples from naive and SIV– or simian HIV–infected PTM. Although PTM MAIT cells generally resemble the phenotype and transcriptional profile of human MAIT cells, they exhibited uniquely low expression of the gut-homing marker α4β7 and were not enriched at the gut mucosa. PTM MAIT cells responded to SIV/simian HIV infection by proliferating and upregulating α4β7, coinciding with increased MAIT cell frequency in the rectum. By 36 wk of infection, PTM MAIT cells were activated and exhibited a loss of Tbet expression but were not depleted as in HIV infection. Our data suggest the following: 1) MAIT cell activation and exhaustion is uncoupled from the hallmark depletion of MAIT cells during HIV infection; and 2) the lack of PTM MAIT cell enrichment at the gut mucosa may prevent depletion during chronic infection, providing a model to assess potential immunotherapeutic approaches to modify MAIT cell trafficking during HIV infection. ***The Journal of Immunology*****, 2019, 202: 2105–2120.**

The population of MR1-restricted mucosal-associated invariant T (MAIT) cells responds to bacterial Ags derived from vitamin B metabolites (1, 2) and/or cytokines such as IL-12, IL-18 (3), and type I IFN (4). Despite their identity as T cells, MAIT cells provide a rapid, innate-like response to both bacterial and viral infections (5), including *Francisella tularensis* (6), *Klebsiella pneumoniae* (7), *Legionella* spp. (8), and influenza (4, 9).

*Department of Microbiology and Immunology, The University of Melbourne, The Peter Doherty Institute for Infection and Immunity, Victoria 3000, Australia; [†]Division of Chemistry and Structural Biology, Institute for Molecular Bioscience, The University of Queensland, Queensland 4072, Australia; [‡]Australian Research Council Centre of Excellence in Advanced Molecular Imaging, The University of Queensland, Queensland 4072, Australia; [§]Melbourne Sexual Health Centre and Department of Infectious Diseases, Alfred Health, Central Clinical School, Monash University, Victoria 3053, Australia; and [¶]Australian Research Council Centre of Excellence in Convergent Bio-Nano Science and Technology, The University of Melbourne, Victoria 3000, Australia

[1]S.B.G.E. and S.J.K. contributed equally to this work.

ORCIDs: 0000-0002-9072-1017 (J.A.J.); 0000-0003-4685-4127 (T.A.); 0000-0001-7368-2979 (B.S.M.); 0000-0002-8011-4539 (J.Y.W.M.); 0000-0002-2693-1896 (L.L.); 0000-0002-7856-8566 (D.P.F.); 0000-0002-8597-815X (J.M.); 0000-0003-0766-171X (S.B.G.E.); 0000-0002-8539-4891 (S.J.K.).

Received for publication October 22, 2018. Accepted for publication January 23, 2019.

This work was supported by National Health and Medical Research Council (NHMRC) Program Grant 1052979. J.A.J. and S.J.K. are funded by NHMRC fellowships. S.B.G.E. is funded by an Australian Research Council fellowship.

Address correspondence and reprint requests to Dr. Jennifer A. Juno, The Peter Doherty Institute for Infection and Immunity, The University of Melbourne, 792 Elizabeth Street, Melbourne, VIC 3000, Australia. E-mail address: jennifer.juno@unimelb.edu.au

The online version of this article contains supplemental material.

Abbreviations used in this article: BAL, bronchoalveolar lavage; B2M, β_2-microglobulin; BV421, Brilliant Violet 421; 6-FP, 6-formylpterin; LN, lymph node; MAIT, mucosal-associated invariant T; MLN, mesenteric LN; NHP, nonhuman primate; OPD, *o*-phenylenediamine dihydrochloride; PTM, pigtail macaque; SHIV, simian HIV; TCID, tissue culture infectious dose.

Given the role of MAIT cells in contributing to immunity against *Mycobacterium tuberculosis* (10, 11) and other opportunistic infections (12), the impact of HIV infection on the MAIT cell population has been a subject of significant interest (13). Multiple studies have demonstrated that both acute and chronic HIV infections result in peripheral MAIT cell depletion that is not fully reversed upon suppressive combination antiretroviral therapy (14–17). Chronic HIV infection is also associated with gut barrier dysfunction and translocation of bacterial products into the circulation (18, 19), which may be the cause of the activated and exhausted phenotype of the remaining MAIT cell population described in human cohorts (17, 20). Thus, the loss and dysfunction of MAIT cells during HIV infection may contribute to an elevated risk of acquiring tuberculosis and other bacterial infections (5, 12).

Despite the insights gained through human cohort studies, numerous questions remain regarding the mechanisms behind the impact of HIV infection on MAIT cells. Because the highly variable levels of MAIT cell preinfection and the timing of HIV acquisition are usually not defined in human cohorts, it is unclear precisely when and why peripheral MAIT cells are lost during infection. It is also unclear whether peripheral blood MAIT cell depletion reflects redistribution of these cells from the circulation to the tissues. More evidence on the mechanism(s) of MAIT activation and exhaustion is required as well as the impact MAIT cell activation may have on viral replication. Studies of MAIT cells in nonhuman primates (NHP) infected with SIV, the best animal model of HIV infection, have been limited to date. Vinton et al. (21) demonstrated a cross-sectional loss of $CD95^+$ MAIT cells in chronically infected rhesus macaques, but no data are available to describe the impact of acute SIV infection on MAIT cell activation or trafficking. Furthermore, recent work has suggested that human MR1 tetramers may exhibit variable

cross-reactivity with NHP MAIT cells, highlighting the usage of species-matched reagents (22).

To study MAIT cell biology in macaque models of HIV infection in more detail, we generated a *Macaca nemestrina* (pigtail macaque [PTM])–specific MR1 tetramer loaded with the MAIT cell Ag 5-OP-RU (23) (MR1–5-OP-RU tetramer). PTM represent a useful model to study MAIT cell biology during HIV-like infections because this model is susceptible to gut barrier dysfunction (24). Using this species-specific MR1 tetramer reagent, we assessed for the first time, to our knowledge, the impact of three different SIV or simian HIV (SHIV) infections on MAIT cell frequency and phenotype in peripheral blood and tissue samples. We find that although PTM MAIT cells are phenotypically and transcriptionally similar to human MAIT cells, they express low levels of the gut-homing marker α4β7 and are rarely detected in the rectal mucosa. During acute SIV/SHIV infection, PTM MAIT upregulate α4β7 as early as 3 wk postinfection and increase in frequency at the rectal mucosa while eventually exhibiting activation and a loss of Tbet expression in the periphery.

Materials and Methods

Animals and viral challenge

Samples collected from juvenile PTMs involved in previous SIV/SHIV challenge trials were included in this study. All animals were purchased from the Australian National Breeding Colony. Samples were selected from animals involved in the following published studies: animals challenged intrarectally with 10^5 tissue culture infectious dose (TCID) $SHIV_{mn229}$ (25) ($n = 4$), animals challenged i.v. with 40 TCID SIV_{mac251} (26) ($n = 4$), and animals challenged i.v. with 2.45×10^7 $SHIV_{SF162P3}$-infected macaque splenocytes in combination with the broadly neutralizing Ab (BnAb) PGT121 or isotype control (27) ($n = 7$). Samples were also selected from $n = 9$ animals ($n = 6$ infected and $n = 3$ uninfected) that were vaccinated with a fowlpox virus/modified vaccinia virus Ankara SIV vaccine or sham vector 98 d prior to challenge with intrarectal challenge with 10^3 $TCID_{50}$ SIV_{mac251}. For longitudinal analysis of mucosal samples (rectal biopsies and bronchoalveolar lavage [BAL]), samples were collected from four animals challenged intrarectally with 10^4 $TCID_{50}$ $SHIV_{SF162P3}$. Characteristics of the animals and viral challenges are reported in Table I. All studies were approved by the The University of Melbourne animal ethics committee.

Viral load and T cell count determination

Plasma SIV and SHIV RNA levels were quantified as previously described (25–27). Whole blood samples were analyzed on a Cell-Dyn Emerald hematology analyzer (Abbott, Chicago, IL), and absolute lymphocyte counts were used to calculate $CD4^+$ T cell and MAIT cell counts using flow cytometry analysis of $CD4^+$ T cell and MAIT cell frequency.

Generation of M. nemestrina *MR1 tetramer*

M. nemestrina MR1 tetramers were generated and characterized as previously described for human and mouse MR1 monomers and tetramers (1, 2, 28). Briefly, *M. nemestrina* genes encoding β_2-microglobulin (B2M) (National Center for Biotechnology Information reference sequence XM_011757352.1) and the soluble portion of MR1 (National Center for Biotechnology Information reference sequence XM_011746239.1) were purchased (Life Technologies Australia), codon optimized for *Escherichia coli* expression. The gene encoding the soluble portion of MR1 was modified to include a mutation to facilitate correct disulphide bond formation, C262S, and to include a C-terminal cysteine for biotinylation using Maleimide-PEG2 biotin (Thermo Fisher Scientific), C272.

The protein sequence of *M. nemestrina* B2M is as follows: MIQRTPKIQVYSRHPPENGKPNFLNCYVSGFHPSDIEVDLLKNGEKMGKVEHSDLSFSKDWSFYLLYYTEFTPNEKDEYACRVNHVTLSGPRTVKWDRDM*. The protein sequence of soluble *M. nemestrina* MR1 is as follows: MRTHSLRYFRLGISDPGHGVPEFISVGYVDSQPITTYDSVTRQKEPRAPWMAENLAPDHWERYTQLLRGWQQTFKVELKRLQRHYNHSGSHTYQRMIGCELLEDGSTTGFLQYAYDGQDFLIFNKDSLSWLAVDNVAHTVKRAWEANQHELRYQKNWLEKECIAWLKRFLEYGNDTLQRTEPPLVRVNRKETFPGVTTLFCKAYSFYPPEIYMTWMKNGEEIVQEMDYGDILPSGDGTYQTWASVELDPKSSNLYSCHVEHS^{262}GVHMVLQVPC^{272}*.

Genes encoding *M. nemestrina* MR1 and B2M were expressed separately in BL21 *E. coli*, and inclusion of body protein was prepared and solubilized in 8 M urea, 20 mM Tris-HCl (pH 8), 0.5 mM Na-EDTA, and 1 mM DTT. MR1 (56 mg per 400 ml folding buffer) and B2M (28 mg per 400 ml folding buffer) were folded in the presence of 6-formylpterin (6-FP; 2 ml per 400 ml folding buffer of a 5 mM solution of powder from Schircks Laboratories, dissolved in water, supplemented with 17 mM NaOH) or 5-amino-6-D-ribitylaminouracil [5-A-RU; 105 μl per 400 ml folding buffer of a 100 mM solution in DMSO generated in house (23)] and methylglyoxal (637 μl per 400 ml folding buffer of a 40% solution from Sigma-Aldrich), respectively by limiting dilution in a buffer adjusted to pH 8–8.5, containing 5 M urea, 100 mM Tris, 2 mM Na-EDTA, 400 mM L-arginine–HCl, 0.5 mM oxidized glutathione, 5 mM reduced glutathione, PMSF, and pepstatin A and dialyzed in 10 mM Tris before fast protein liquid chromatography purification by sequential DEAE anion exchange, gel filtration, and Mono-Q anion exchange chromatography. Purified protein was then reduced with 25 mM DTT for 15 min before buffer exchange into PBS using a PD-10 column (GE Healthcare). The cysteine-tagged MR1–5-OP-RU and MR1–6-FP monomers were biotinylated with Maleimide-PEG2 biotin (Thermo Fisher Scientific) with a 30:1 M ratio of biotin reagent to protein at 4°C for 16 h in the dark and subjected to Mono-Q anion exchange chromatography to eliminate free biotin and isolate biotinylated MR1–5-OP-RU and MR1–6-FP monomers. Biotinylated MR1–5-OP-RU and MR1–6-FP monomers were stored at −80°C. For tetramerization, aliquots were thawed out and tetramerized with streptavidin conjugated to PE (BD Biosciences) or Brilliant Violet 421 (BV421; Invitrogen) at a 8:1 M ratio of MR1 to streptavidin–fluorochrome to a final concentration of 143 ng/μl.

ELISA to characterize biotinylated MR1 monomers

Ninety-six–well U-bottom plates (Nunc-Immuno plate; Thermo Fisher Scientific) were coated with streptavidin at 1 μg in PBS per 100 μl well overnight at 4°C. Wells were then washed four times with 0.1% Tween/PBS, blocked with 200 μl 1% BSA/PBS for 1 h at 37°C, and washed again three times with 0.1% Tween/PBS. One hundred microliters per well of 2-fold serial dilutions of biotinylated MR1 monomers in 1% PBS/BSA was added. Following incubation for 1 h at 37°C, wells were washed five times with 0.1% Tween/PBS prior to the addition of 1 μg per well of primary Ab 26.5 or isotype control 8A5 (isotype IgG2a), and Ab 8F2.F9 or isotype control 3E12 (isotype IgG1), respectively in 1% BSA/PBS. All Abs were produced in house. The hybridomas of 26.5 (29) and 8F2.F9 (30) were a gift from T. Hansen (University of Washington) and W.J. Yankelevich (U.S. Food and Drug Administration). 8A5 is specific for the human pre-TCR α-chain and 3E12 is specific for HLA-B*57 and HLA-B*58 members of the HLA-B17 serogroup (31). The experiment was incubated for 1 h at 37°C, and wells were washed four times with 0.1% Tween/PBS. Then polyclonal goat anti-mouse HRP-conjugated Ab (Abcam) as enzyme-linked secondary Ab was added at a 1:2000 dilution in 150 μl 1% BSA/PBS and the plate was incubated for 1 h at 37°C. Wells were then washed four times with 0.1% Tween/PBS, and an HRP-dependent substrate reaction using *o*-phenylenediamine dihydrochloride (OPD; Sigma-Aldrich) was carried out as follows: an OPD tablet was dissolved in 25 ml of OPD phosphate-citrate buffer, and 10 μl of 30% H_2O_2 were added and the solution mixed. One hundred and fifty microliters of OPD substrate solution was added per well and incubated at room temperature. OPD substrate turnover was stopped using 50 μl of 2.25 M HCl once an orange-brown color had developed, and the plate was analyzed spectrophotometrically at 492 nm using a Multiskan Ascent multiwell plate reader (Thermo Electron). Data were analyzed using GraphPad Prism 7 (GraphPad), whereby EC_{50} values were determined upon baseline correction, normalization, and nonlinear curve fitting.

Blood and tissue processing

PBMCs were isolated from heparin- or EDTA-treated whole blood samples by Ficoll gradient. Cells were cryopreserved in 90% FCS/10% DMSO (freezing media) and stored in liquid nitrogen until analysis.

Liver, spleen, and thymus samples were diced into small pieces and passed through a 70-μm strainer to produce a single-cell suspension. The suspension was washed twice in RPMI 1640 media with 10% FCS (RF10) and cryopreserved in freezing media. Mesenteric and inguinal lymph nodes (LN) were isolated by removing the LN capsule and collecting the cells in RF10. Samples were strained through a 70-μm filter, washed, and cryopreserved in freezing media.

BAL samples were obtained by aspirating saline flushed into the lungs through a flexible feeding tube placed laryngoscopically. Samples were transported on ice and centrifuged at 500 × *g* for 5 min, and the cell pellet was resuspended in RF10. The cell suspension was filtered through a 30-μm

filter, and the filtrate was immediately collected for staining with Abs for flow cytometry. Rectal biopsies were collected by using pinch biopsy forceps placed 5 cm into the rectum. Samples were transported on ice. Biopsy tissues were washed in RPMI 1640 and incubated in digestion buffer (0.1 mg/ml collagenase and 1.5 U/ml DNase in RF10) at 37°C for 2 h. The buffer and remaining tissue samples were passed through a 70-μm filter and washed in RF10. The resulting cell pellet was resuspended in RF10 and passed through a 30-μm cell filter, then transferred immediately for Ab staining and flow cytometry.

Cell culture and stimulation

Cryopreserved PBMC or single-cell suspension tissue samples were thawed and, if appropriate, cultured in RF10 media with penicillin, streptomycin, and glutamine (Life Technologies) at 37°C. Mitogenic stimulation was performed by incubating PBMC in the presence of PMA (Sigma-Aldrich) and ionomycin (Sigma-Aldrich) for 6 h, with GolgiStop and GolgiPlug (BD Biosciences) added for the final 4 h of incubation. Evaluation of CD69 upregulation by 5-OP-RU [generated in house (23)] and 6-FP Ags was performed in fresh PBMC for 6 or 16 h by incubating cells with no Ag (unstimulated), 100 μM 6-FP, or 1 or 10 nM 5-OP-RU. Quantification of proliferation was performed by loading freshly isolated PBMC with CellTrace Violet (Thermo Fisher Scientific) according to the manufacturer's instructions, stimulating cells with 10 nM 5-OP-RU (with an unstimulated control) and culturing cells in RF10 supplemented with 100 IU/ml human rIL-2 (PeproTech) for 4–6 d. Ag-specific MAIT cell stimulation for cytokine quantification was carried out after thawed PBMC were rested for 6 h, at which time they were stimulated with 10 nM 5-OP-RU for 16 h. GolgiStop and GolgiPlug were added 1 h into the incubation. In some cases, cells were stimulated with 5-OP-RU in media containing 50 ng/ml rhesus macaque rIL-12 and rIL-18 proteins (R&D Systems).

Cell staining and flow cytometry

For staining of surface markers, 2×10^6 thawed cells were collected, washed, and incubated with a 1:800 or 1:1000 dilution of stock MR1 tetramer at room temperature for 5–10 min. A mixture of surface Abs was then added and incubated with cells for 30 min at 4°C. Where indicated, cells were permeabilized with BD Cytofix/Cytoperm (BD Biosciences) as recommended by the manufacturer and stained intracellularly for cytokine expression. Transcription factor and Ki67 staining was performed using the BD Transcription Factor Staining Buffer (BD Biosciences), followed by incubation with intracellular Abs. Quantification of CD107a expression was performed by adding anti-CD107a Ab during cell culture and stimulation. A complete list of Abs used in flow experiments is provided in Table II. The anti-α4β7 Ab used in this study was provided by the National Institutes of Health Nonhuman Primate Reagent Resource (R24 OD010976, U24 AI126683). Cells were acquired on a BD LSR Fortessa using BD FACSDiva software. A minimum of 400,000 lymphocyte events were collected. Flow data were analyzed using FlowJo v10.2 (TreeStar). Gating for PBMC and tissues is indicated in Supplemental Fig. 1A. Gates were set based on fluorescence minus one controls (Supplemental Fig. 1B).

Statistical analysis

Statistical analyses were performed using GraphPad Prism 7 (GraphPad). Two group comparisons were performed using the Mann–Whitney *U* (unpaired) or Wilcoxon matched-pairs test (paired data). Three or more group comparisons were performed using Kruskal–Wallis (unpaired) or Friedman test (paired), followed by Dunn or Tukey posttest, respectively. Correlations were performed by Spearman test. The p values <0.05 were considered significant.

Results

Generation and characterization of M. nemestrina*–specific MR1 monomers*

Studies in rhesus macaques suggest human MR1 tetramers may be only partially cross-reactive with macaque MAIT cells (22), but no detailed studies have been performed in pigtailed macaques. Biotinylated *M. nemestrina* MR1 monomers loaded with 5-OP-RU and 6-FP were generated as described previously for human and mouse MR1 monomers (1, 2, 28). When assessed by gel electrophoresis, *M. nemestrina* MR1 monomers were composed of species with molecular weights as expected for MR1 and B2M and were of high purity, similar to human biotinylated MR1 monomers (Supplemental Fig. 2A). MR1 is highly conserved across species, with only 10 aa differences between human and macaque MR1 α1 and α2 domains (Supplemental Fig. 2B, 2C). Thus, we suspected that the conformation-dependent Ab clone 26.5, specific for human MR1 and cross-reactive with mouse MR1 (29), and the conformation-dependent (32) Ab clone 8F2.F9, specific for mouse MR1 and cross-reactive with rat, bovine, and human MR1 (30), might also bind to macaque MR1 in a conformation-dependent manner and could be used to assess the fold of the newly generated biotinylated macaque MR1 monomers. Indeed, both 26.5 and 8F2.F9 Abs (Supplemental Fig. 2D), but not isotype controls (Supplemental Fig. 2E), bound macaque MR1–5-OP-RU and macaque MR1–6-FP in a dose-dependent manner in ELISA with EC_{50} values similar to those observed for human and mouse MR1 monomers (Supplemental Fig. 2F). In summary, we generated biotinylated macaque MR1 monomers that from a biochemical perspective appeared suitable for studying macaque MAIT cells by flow cytometry in their tetrameric fluorochrome-tagged version.

Identification of M. nemestrina *5-OP-RU–specific T cells in peripheral blood using* M. nemestrina*–specific MR1 tetramer*

In humans, MR1–5-OP-RU tetramer identifies 5-OP-RU–reactive MAIT cells that are largely TRAV1-2$^+$, although TRAV1-2$^-$ MR1-tetramer$^+$ cells have been observed at low frequencies (33), whereas MR1–6-FP tetramers often serve as a control given that most MR1-restricted T cells do not stain with MR1–6-FP tetramer (34). Costaining of PTM PBMC with the human Vα7.2-specific mAb 3C10 [known to cross-react with macaque Vα7.2 (22)], and macaque MR1–6-FP tetramer resulted in background levels of tetramer staining (Fig. 1A). In contrast, macaque MR1–5-OP-RU tetramer identified in a dose-dependent manner a population of T cells that was also Vα7.2$^+$, consistent with the macaque MR1 tetramer staining being 5-OP-RU–Ag specific (Fig. 1A, Supplemental Fig. 3A). The frequency of Vα7.2$^+$tetramer$^+$ cells ranged from 0.026 to 1.28% (median 0.25%) of CD3$^+$ T cells among 33 naive animals.

Addition of the MR1–5-OP-RU tetramer prior to staining with the Vα7.2 mAb demonstrated competition for TCR binding between the two reagents (Supplemental Fig. 3B), further highlighting the specificity of the tetramer. Additionally, a subset of Vα7.2$^+$ cells stained with MR1–5-OP-RU tetramer regardless of whether a PE or BV421 fluorochrome streptavidin conjugate was used for tetramerization (Supplemental Fig. 3C, 3D). Interestingly, the macaque MR1–5-OP-RU tetramer also stained variable proportions of Vα7.2$^-$ T cells. Whereas tetramer staining of Vα7.2$^+$ cells was robust over more than two logs of tetramer dose, Vα7.2$^-$ MR1–5-OP-RU tetramer$^+$ cells were only identified over one log of tetramer dose (Supplemental Fig. 3A, 3E). The frequency of Vα7.2$^-$ MR1–5-OP-RU tetramer$^+$ cells was $<0.03\%$ of T cells in some animals at dilutions as high as 1:800 (Supplemental Fig. 3E, 3F), consistent with an Ag-dependent low-avidity interaction between Vα7.2$^-$ TCRs and MR1–5-OP-RU tetramer. Given the distinct staining pattern as well as the absence of Vα7.2$^-$ MR1–5-OP-RU tetramer$^+$ cells in some of the PTM samples, we only considered Vα7.2$^+$ MR1–5-OP-RU tetramer$^+$ cells for the remainder of this study.

Given discrepancies between the reported cross-reactivity of human MR1 tetramers with macaque MAIT cells (21, 22), we compared the binding of PTM and human MR1 tetramers on naive PTM PBMC. Both species' 6-FP–loaded tetramers showed similar levels of background staining (Supplemental Fig. 3G). The 5-OP-RU–loaded PTM tetramer appeared to have higher affinity for PTM MR1-restricted T cells compared with the human tetramer, as a 4-fold greater concentration of human tetramer was needed to identify a tetramer$^+$Vα7.2$^+$ T cell population that was comparable to that of the PTM tetramer (Supplemental Fig. 3H). At this

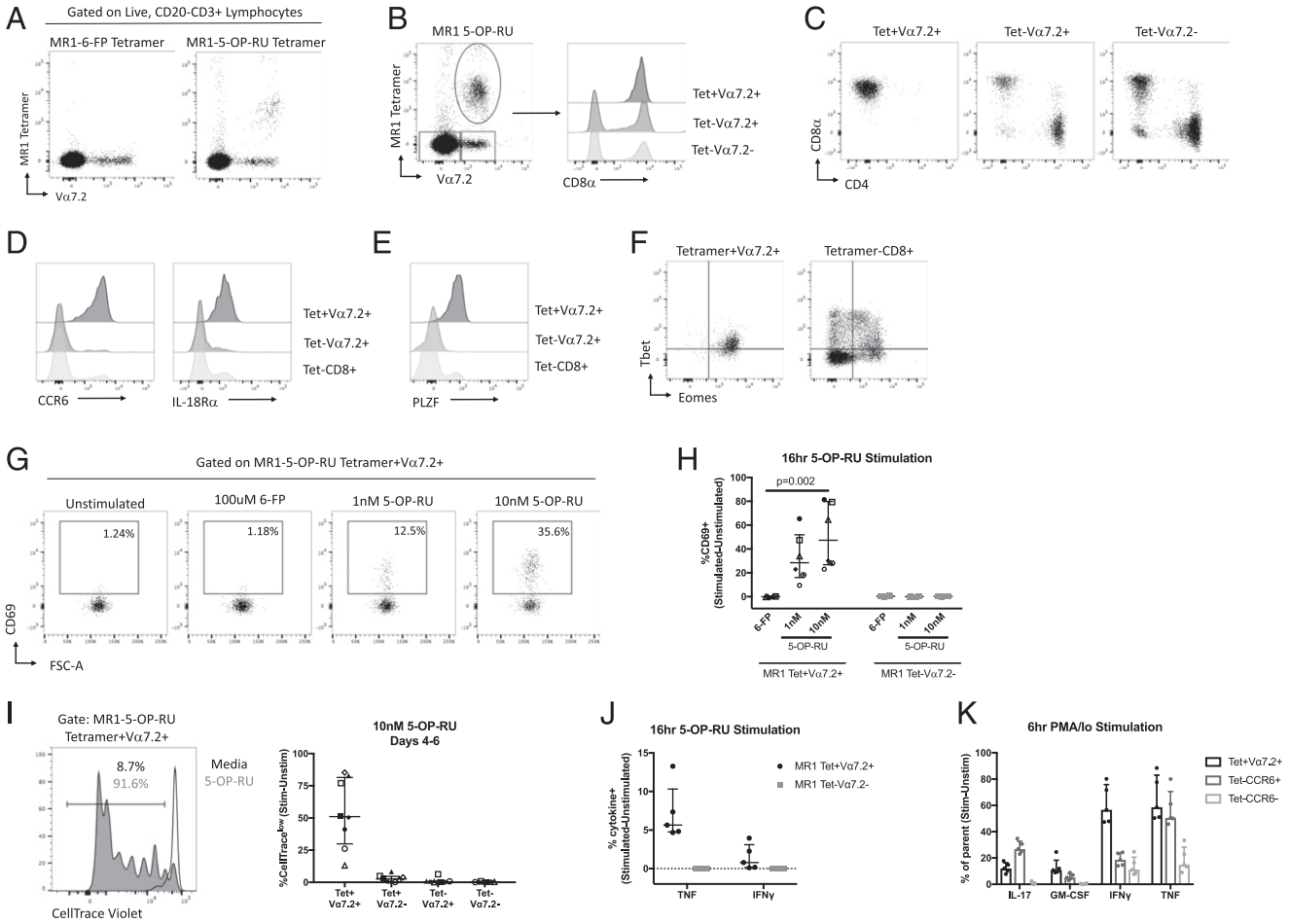

FIGURE 1. Characterization of macaque MR1–5-OP-RU tetramer-reactive T cells. (**A**) Representative staining of *M. nemestrina* PBMC with 6-FP or 5-OP-RU–loaded MR1 tetramer. Lymphocytes were identified by forward scatter (FSC) and side scatter (SSC), followed by FSC area versus height gating to exclude doublets. Live, CD20-CD3$^+$ cells were then assessed for MR1 tetramer binding and TCR Vα7.2 expression. (**B**) Comparison of CD8a and (**C**) CD4 coreceptor expression between MR1 tetramer$^+$Vα7.2$^+$, MR1 tetramer$^-$Vα7.2$^+$, and MR1 tetramer$^-$Vα7.2$^-$ T cells. MR1 tetramer-reactive T cells were also assessed for expression of (**D**) CCR6 and IL-18Ra, (**E**) PLZF, and (**F**) Tbet and Eomes compared with MR1 tetramer$^-$Vα7.2$^+$ and MR1 tetramer$^-$CD8$^+$ T cells. Results are representative of 18 naive macaques. (**G**) Fresh PBMC were cultured in the presence of 100 μM 6-FP, 1 or 10 nM 5-OP-RU, or left unstimulated for 16 h. Plots show representative staining of CD69 expression on MR1 tetramer$^+$Vα7.2$^+$ MAIT cells in each condition for one of five animals. (**H**) Quantification of CD69$^+$ MAIT cells or MR1 tetramer$^-$Vα7.2$^-$ cells after background subtraction of unstimulated CD69 expression. Symbols identify individual animals (n = 5 naive animals). (**I**) Fresh PBMC were loaded with CellTrace Violet, stimulated with 10 nM 5-OP-RU, and cultured for 4–6 d in RF10 supplemented with 100 IU/ml human rIL-2. Plot shows CellTrace dilution among the MR1–5-OP-RU tetramer$^+$Vα7.2$^+$ gate following 5-OP-RU stimulation or media control for one animal. Graph indicates background subtracted proportions of CellTrace^{low} cells for MR1 tetramer/Vα7.2 coexpressing populations (n = 8 naive macaques). Each symbol represents paired data from one animal. (**J**) Macaque PBMC were stimulated for 16 h with 10 nM 5-OP-RU and assessed for expression of TNF and IFN-γ. Graphs show comparison of 10 nM 5-OP-RU reactivity between MAIT cell and MR1 tetramer$^-$Vα7.2$^-$ cells (n = 5 naive animals). (**K**) Previously cryopreserved macaque PBMC were stimulated for 6 h with PMA and ionomycin. Graph indicates proportions of IL-17$^+$, GM-CSF$^+$, TNF$^+$, and IFN-γ$^+$ cells in the MR1 tetramer$^+$Vα7.2$^+$ MAIT cell gate or CD3$^+$tetramer$^-$CCR6$^+$ or CCR6$^-$ T cells. Lines and error bars on graphs indicate median ± interquartile range. Statistics assessed by Friedman test with Dunn posttest.

concentration, the human tetramer identified a slightly lower proportion of tetramer$^+$Vα7.2$^+$ cells than the PTM tetramer, possibly because of low tetramer staining on some Vα7.2$^+$ cells (Supplemental Fig. 3I). As a control, we confirmed that staining of human PBMC with the human tetramer clearly identified Vα7.2$^+$ MAIT cells (Supplemental Fig. 3J). Costaining with Vα7.2 and human and PTM 5-OP-RU tetramers confirmed that both reagents generally identify the same cells but that the PTM tetramer can out-compete the human tetramer for binding to a subset of Vα7.2$^+$ cells (Supplemental Fig. 3K). Overall, these results suggest that whereas the human MR1 tetramer exhibits cross-reactivity with PTM T cells, the species-matched reagent is preferable for the specific and accurate identification of PTM MR1-restricted T cells, particularly in the context of disease where MAIT cell activation might result in lower levels of surface TCR expression.

Assessment of canonical MAIT cell surface marker and transcription factor expression in PTM MR1 tetramer-reactive T cells

Guided by markers characteristic for human MAIT cells, we characterized PTM Vα7.2$^+$ MR1–5-OP-RU tetramer$^+$ cells. This excluded consideration of CD161 expression, as we confirmed previous observations (22) that even with the brightest fluorochromes, CD161 detection using the human Ab HP-3G10 was poor in PTM (data not shown). Vα7.2$^+$ MR1–5-OP-RU tetramer$^+$ cells were primarily CD8α$^+$ (Fig. 1B, 1C) and notably did not include the CD4$^-$CD8$^-$ MAIT cell subset that is observed in

humans (35). The PTM Vα7.2$^+$ MR1–5-OP-RU$^+$ cells were also uniformly CCR6$^+$ and IL-18Ra$^+$, exhibiting a distinct phenotype from both the conventional CD8$^+$ T cell population and the MR1–5-OP-RU tetramer$^-$Vα7.2$^+$ subset (Fig. 1D). The expression of key transcription factors in PTM Vα7.2$^+$ MR1–5-OP-RU tetramer$^+$ T cells was also strikingly similar to that of human MAIT cells; they are uniformly PLZF-expressing, and the majority displayed a Tbet^{dim}Eomes$^+$ phenotype (Fig. 1E, 1F). Thus, based on Ag specificity, surface markers and transcription factors, macaque MR1–5-OP-RU tetramer in combination with Vα7.2 mAb staining identifies a population of cells that is consistent with MAIT cells as previously described in humans, which we will refer to in this study as PTM MAIT cells.

Confirmation of PTM MAIT cell 5-OP-RU Ag reactivity

We next tested if MR1–5-OP-RU tetramer$^+$Vα7.2$^+$ macaque MAIT cells also responded to 5-OP-RU in vitro. After culture of fresh PBMC with 5-OP-RU or 6-FP for 16 h, we observed a dose- and Ag-dependent upregulation of CD69 on PTM MAIT cells but not MR1 tetramer$^-$Vα7.2$^-$ cells to a maximum of ~80% in some animals (Fig. 1G, 1H). Similarly, culture of PBMC for 4–6 d following 5-OP-RU stimulation resulted in selective proliferation of the MR1 tetramer$^+$Vα7.2$^+$ T cell population (Fig. 1I). Despite robust CD69 and proliferative responses, PTM MAIT cells exhibited relatively low cytokine secretion following 5-OP-RU stimulation (Fig. 1J), although the secretion of IFN-γ could be augmented by the inclusion of macaque rIL-12 and rIL-18 during 5-OP-RU stimulation (data not shown). Following mitogenic stimulation with PMA/ionomycin for 6 h, however, PTM MAIT cells expressed high levels of TNF and IFN-γ, as well as moderate levels of IL-17 and GM-CSF (Fig. 1K).

Characterization of PTM MAIT cell tissue homing and activation

Human MAIT cells predominately exhibit a tissue-homing phenotype and are enriched in many mucosal and non-mucosal tissues (36), but the expression of tissue-homing markers other than CCR6 and CCR7 on NHP MAIT cells is limited. Analysis of PTM MAIT cell phenotype relative to conventional CD8$^+$ T cells revealed many similarities to human MAIT cells, with several notable differences. In addition to the uniform expression of CCR6, macaque MAIT cells expressed high levels of CCR5 and were uniformly CXCR3$^+$ (Fig. 2A). In contrast to human MAIT cells, which ubiquitously express the mucosal homing integrin α4β7 (37), only a minority of circulating macaque MAIT cells are α4β7$^+$ (median 12.9% α4β7$^+$ across 12 PTM), a frequency significantly lower than that in the conventional CD8$^+$ T cell population (median 48.2% α4β7$^+$, $p = 0.0005$; Fig. 2A). Similar to other studies (38, 39), conventional T cell α4β7^{mid} and α4β7^{hi} populations were clearly defined (Fig. 2B), including the HIV/SIV-susceptible CD4$^+$α4β7^{hi}CCR6$^+$ Th17 population (39), ruling out a global T cell α4β7 defect in these animals.

As expected given the high MAIT cell expression of chemokine receptors, we detected an enrichment of MAIT cells in the liver and lung relative to the peripheral blood (Fig. 2C; gating shown in Supplemental Fig. 1). MAIT cells were less abundant in the spleen and mesenteric and inguinal LN compared with PBMC and were infrequently found in the thymus (Fig. 2D). Strikingly, we consistently observed only low frequencies of MAIT cells in the rectal mucosa of naive animals (Fig. 2E). The apparent lack of MAIT cell enrichment in the gut/rectum is consistent with the low ex vivo MAIT cell α4β7 expression we observed in PTM but stands in contrast to studies in humans, which have previously reported higher median MAIT cell frequencies in the rectum or colon relative to peripheral blood (17, 40).

In the periphery, PTM MAIT cells expressed low levels of the activation markers CD69 and HLA-DR, similar to the bulk CD8$^+$ T cell population; in contrast, the majority of MAIT cells expressed PD-1 (median 61.3% PD-1$^+$; Fig. 2F). PD-1 expression on PTM MAIT cells was distinct to that of both conventional PTM CD8$^+$ T cells (Fig. 2F) and human MAIT cells [data not shown and (41)]. Blockade of PD-1 during 5-OP-RU stimulation did not alter MAIT cell cytokine responses, suggesting that high PD-1 expression does not inhibit MAIT cell activation in naive animals (data not shown). Despite the low levels of peripheral MAIT activation, CD69 was highly expressed on tissue-derived MAIT cells (Fig. 2G), likely reflecting the role of CD69 as a tissue retention marker on human T cells.

Acute SIV/SHIV infection leads to MAIT cell upregulation of α4β7

To assess the impact of acute and early chronic MAIT cell response to SIV/SHIV infection in PTMs, cryopreserved samples were studied from previous SIV/SHIV infection studies (Table I). Animals were infected with one of three viruses: SIV_{mac251} (CCR5-tropic), $SHIV_{SF162P3}$ (CCR5-tropic), or $SHIV_{mn229}$ (CXCR4-tropic, highly pathogenic), and followed for as long as 81 wk postchallenge (SIV_{mac251} infection). Where possible, we compared infected animals to controls that were protected from SIV or SHIV infection in the same trials by vaccination or Ab infusions. MAIT cell phenotype was assessed based on expression of surface markers and transcription factors as shown in Figs. 1, 2, Supplemental Fig. 1, and as listed in Table II. Viral load and CD4 counts of chronically infected animals are shown in Supplemental Fig. 4A, 4B.

Longitudinal analysis of MAIT phenotype during acute SIV/SHIV infection (in animals with detectible viremia at week 1 postchallenge) revealed that most animals exhibited a transient increase in MAIT cell α4β7 expression at week 3 or 4 postchallenge (Fig. 3A, 3B) that occurred regardless of viral tropism or route of infection (Fig. 3B). Whereas MAIT cell α4β7 expression increased almost 2-fold by weeks 3–4 postchallenge (median 15.3% α4β7$^+$ at baseline versus 29.6% α4β7$^+$ at week 3–4, $p < 0.0001$, Fig. 3C), conventional CD8$^+$ T cell α4β7 expression decreased slightly during the same timespan (median 60.8% α4β7$^+$ at baseline versus 54.3% α4β7$^+$ at week 3–4, $p = 0.036$). In animals infected with a CCR5-tropic virus [in which α4β7^{hi} Th17 CD4$^+$ T cells are preferential HIV/SIV target cells (42)], animals exhibited progressive loss of α4β7^{hi}CCR6$^+$ CD4$^+$ T cells (data not shown). In contrast to the modulation of α4β7, expression of other chemokine receptors and activation markers such as CCR5, CCR6, CXCR3, CD69, and HLA-DR on MAIT cells was unperturbed by infection (data not shown).

The cohort of animals challenged intrarectally with $SHIV_{SF162P3}$ was large enough to conduct exploratory correlations between MAIT cell frequency, changes in α4β7 expression, and early viral load kinetics. In a total of 10 animals (eight with viremia at week 1 and two with delayed viremia), the change in MAIT cell α4β7 expression at week 3 correlated with both week 3 viral load and the peak viral load (Fig. 3D, $p = 0.005$ and 0.003, respectively), suggesting that early viral replication may drive the change in MAIT phenotype. Baseline MAIT cell frequency weakly correlated with viral load at week 3 (Fig. 3D, $p = 0.052$), suggesting that preinfection peripheral MAIT cell frequency did not play a substantial regulatory or protective role during early infection.

Changes in MAIT cell α4β7 expression are associated with Ag exposure and MAIT cell recruitment to the rectum

In humans and mice, induction of α4β7 on conventional T cells is mediated by retinoic acid–producing mesenteric LN (MLN) or

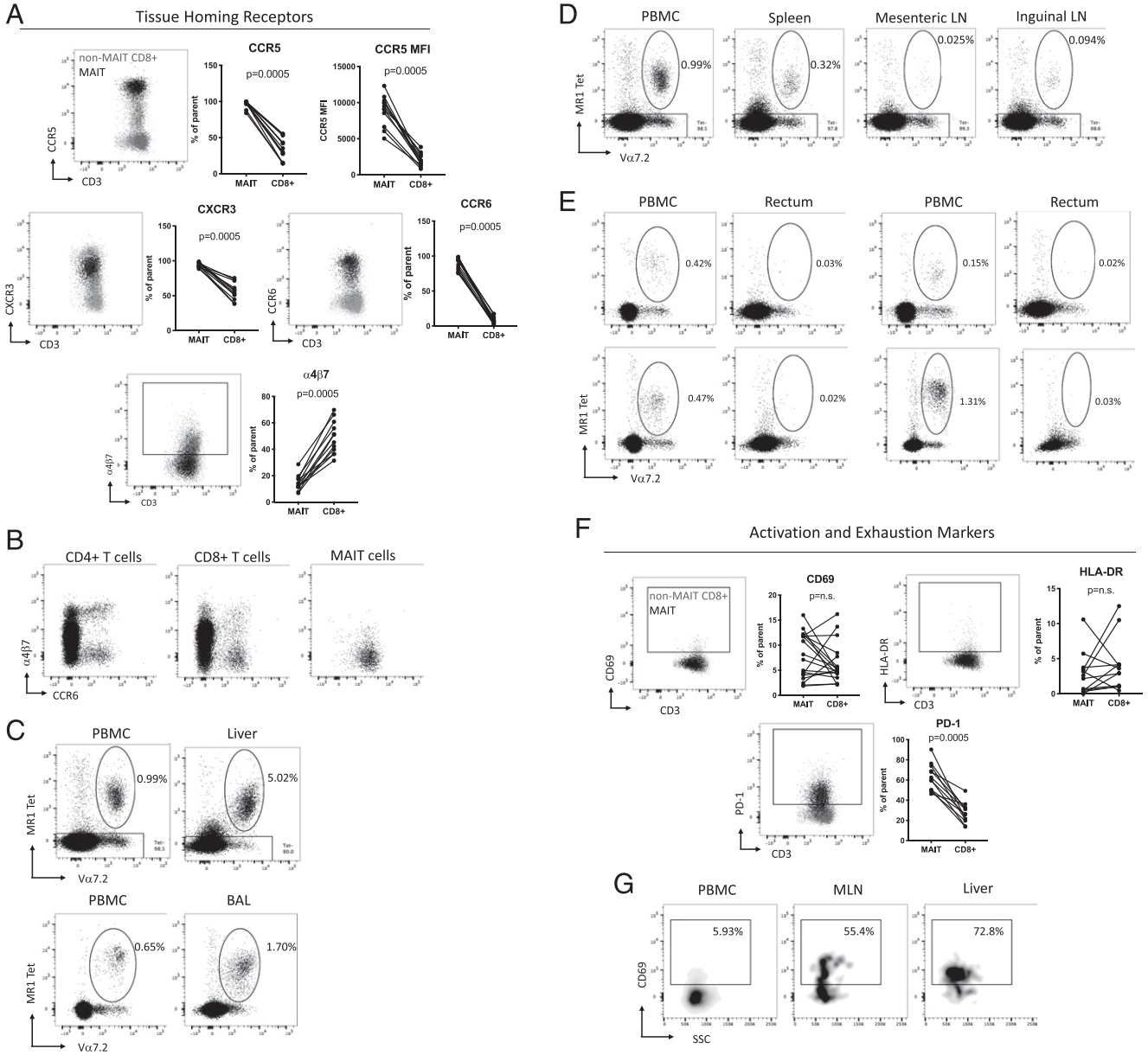

FIGURE 2. MAIT cell tissue phenotype and tissue distribution. (**A**) Expression of tissue-homing markers CCR5, CXCR3, CCR6, and α4β7 on peripheral blood MAIT cells from naive macaques. Plots show MAIT cell gate (black) and conventional $CD8^+$ T cell gate (gray). Statistical comparison of surface marker frequency or mean fluorescence intensity (MFI) performed by Wilcoxon test (n = 12). (**B**) Representative coexpression of α4β7 and CCR6 on $CD4^+$, $CD8^+$, or MAIT cells. (**C**) Representative MAIT cell frequencies in matched cryopreserved PBMC/liver or freshly stained PBMC/BAL samples from naive macaques. (**D**) Representative MAIT cell frequencies in matched cryopreserved PBMC, spleen, inguinal LN, and MLN samples from a naive macaque. (C and D) Plots are representative of samples from n = 4–6 SIV/SHIV-uninfected animals. (**E**) MAIT cell frequencies in matched cryopreserved PBMC/rectal biopsy samples from four naive macaques (derived from three independent experiments). Plots are representative of 15 naive macaques sampled in five independent experiments. (**F**) Expression of activation/exhaustion markers CD69, HLA-DR, and PD-1 on peripheral blood MAIT cells from naive macaques. Plots show MAIT cell gate (black) and conventional $CD8^+$ T cell gate (gray). Statistical comparison of surface marker frequency or MFI performed by Wilcoxon test (n = 18 for CD69, n = 12 for HLA-DR, PD-1). (**G**) Density plots are representative of MAIT cell CD69 expression in the MLN and liver relative to PBMCs.

Peyer patch–derived dendritic cells in the presence of Ag (38, 43–45). Stimulation of PBMC with 5-OP-RU resulted in only low levels of α4β7 upregulation compared with a media control (Fig. 4A; median 16.15% $\alpha4\beta7^+$ versus 11.2% $\alpha4\beta7^+$ in media alone). In contrast, coculture of autologous PTM MLN lymphoid cells with PBMC in the presence 5-OP-RU resulted in a substantially stronger induction of α4β7 on MAIT cells (from a median of 8.1–25.6%; Fig. 4B), suggesting that MAIT cell α4β7 upregulation during SIV/SHIV infection may be related to increased Ag availability in the LN. Coculture and stimulation resulted in no change in conventional $CD8^+$ T cell α4β7 expression (Fig. 4B). The ability of 5-OP-RU to induce MAIT cell α4β7 expression was not compromised by SHIV infection, as similar levels of upregulation were observed in cell culture from both uninfected and $SHIV_{SF162P3}$-infected animals.

We hypothesized that if α4β7 expression does regulate MAIT cell trafficking to the gut and rectal mucosa, MAIT cell frequency in rectal biopsies should increase at week 3 postinfection. Biopsies from

Table I. Characteristics of animals in SIV/SHIV challenge studies

Virus Challenge	Challenge Dose	Challenge Route	Animal ID	Weeks Studied[a]	Plasma Viremia	Peak Viral Load	Setpoint Viral Load[b]	Tissues Analyzed[c]	Week of Necropsy[d]	Notes	Publication
$SHIV_{SF162P3}$	10^4 $TCID_{50}$	IR	E60D	0–14	Y	8.15	ND	Rectum, BAL			M.S. Parsons,
			O390	0–14	Y	8.04	ND	Rectum, BAL			A.B. Kristensen,
			4499	0–14	Y	7.41	ND	Rectum, BAL			K.J. Selva, T. Amarasena,
			2755	0–14	Y	6.64	ND	BAL			J.A. Juno, H.X. Tan,
			CD46	0–14	Y	5.28	ND			Viremia week 3	R.E. Esterbauer, A. Wheatley,
			01DE	0–14	Y	6.86	ND			Viremia week 2	B.R. Bavinton, A.E. Grulich,
			BABD	0–5	Y	7.92	ND				A.D. Kelleher, G. Khoury,
			CF6C	0–5	Y	8.49	ND				and S.J. Kent, manuscript
			C8CC	0–5	Y	8.20	ND				in preparation
			95A7	0–5	Y	7.84	ND				
SIV_{mac251}	40 TCID	i.v.	9175	0–73	Y	6.16	3.47			Antiretroviral therapy	De Rose et al. 2008 (26)
			9196	0–73	Y	6.43	3.54			administered weeks	
			8020	1–73	Y	7.09	4.17			3–10	
			8251	1–73	Y	7.87	4.72				
SIV_{mac251}	10^3 $TCID_{50}$	IR	A50D	0–35	Y	7.32	6.06	Y	Week 35		M. Khanna, R.J. Jackson,
			A730	0–35	Y	7.26	5.92	Y	Week 35		S. Alcantara,
			B68D	0–18	Y	7.73	6.47	Y	Week 18		T.H. Amarasena, Z. Li,
			CE71	0 and 35	Y	7.87	6.77	Y	Week 35		A.D. Kelleher, S.J. Kent,
			D2CD	0 and 22	Y	8.03	7.14	Y	Week 22		and C. Ranasinghe,
			55A3		N	N/A	N/A	Y		Protected by Fowlpox- and	submitted for publication
			94D5		N	N/A	N/A	Y		MVA-SIV vaccination	
			AAB5		N	N/A	N/A	Y			
$SHIV_{SF162P3}$	2.45×10^7 infected splenocytes	i.v.	658D	0–16	Y	6.11	5.03	Y	Week 16		Parsons et al. 2017 (27)
			D77C	0–27	Y	6.84	5.67	Y	Week 27		
			FACA	0–81	Y	6.90	4.50			Controlled infection after week 59	
			F2F0	0–40	Y	6.22	N/A			Controlled infection after week 6	
			DEF1		N	N/A	N/A			Protected by PGT121	
			8DF8		N	N/A	N/A	Y		BnAb infusion	
			4B31		N	N/A	N/A				
$SHIV_{mn229}$	10^5 TCID	IR	6262	0–22	Y	6.94	5.54				De Rose et al. 2007 (25)
			6349	0–24	Y	7.23	5.77				
			6363	0–11	Y	7.69	5.96				
			6377	0–11	Y	7.66	5.71				

[a]SIV/SHIV–infected animals only; not all samples were available for all phenotypic analyses.
[b]SIV_{mac251} i.v. challenge: mean weeks 12–20 (post-ART discontinued); SIV_{mac251} IR challenge: mean weeks 4–10; $SHIV_{SF162P3}$: mean weeks 4–11; SIV_{mn229}: mean weeks 4–11.
[c]Spleen, liver, MLN, inguinal LN, and thymus samples collected and cryopreserved at necropsy.
[d]SIV/SHIV–infected animals only.
BnAb, broadly neutralizing Ab; ID, identifier; IR, intrarectal; MVA, modified vaccinia virus Ankara; N, no; N/A, not applicable; Y, yes.

Table II. Abs used for flow cytometry

Marker	Clone	Color	Use
CD3	SP34-2	Alexa700	Lineage
CD4	L200	BV605	T cell subsets
CD8	RPA-T8	BV650	T cell subsets
Vα7.2	3C10	BV510/allophycocyanin/BV421	MAIT cell identification
CD20	2H7	PE-CF594	Lineage
Vδ1	TS8.2	FITC	γ δ T cell exclusion
Vδ2	15D	FITC	γ δ T cell exclusion
CCR6	G034E3	BV785	MAIT phenotype
CCR5	J418F1	BV421	MAIT phenotype
CXCR3	G02H57	PE-Dazzle 594	MAIT phenotype
α4β7	α4β7 (NIH)	Allophycocyanin	MAIT phenotype
IL-18Ra	H44	Allophycocyanin	MAIT phenotype
CD69	FN50	Allophycocyanin–fire 750	MAIT activation
HLA-DR	L243	Allophycocyanin–fire750	MAIT activation
PD-1	EH12.2H7	BV421	MAIT exhaustion
CD161	HP-3G10	BV421	MAIT identification
CD107a	H4A3	Allophycocyanin-H7	MAIT degranulation
Ki67	B56	BUV395	Proliferation
Tbet	4B10	BV421	Transcription factor
Eomes	WD1928	PE-eFluor610	Transcription factor
PLZF	R17-809	Alexa647	Transcription factor
IFN-γ	B27	BUV395	Cytokine production
TNF	MAb11	Allophycocyanin-Cy7	Cytokine production
IL-17	BL168	BV605	Cytokine production
GM-CSF	BVD2-21C11	BV421	Cytokine production
CD45	D058-1283	BUV395	Lineage (tissues)
EpCam/CD326	EBA-1	PE-CF594	Epithelial cell exclusion (tissues)

three animals infected with $SHIV_{SF612P3}$ demonstrated an increase in MAIT cell frequency at week 3 postinfection compared with week 1 or week −5 (Fig. 4C), which declined from weeks 5 to 14, but remained elevated above baseline (Fig. 4D). Additionally, unmatched samples from a separate cohort of eight uninfected animals and three $SHIV_{SF612P3}$-infected animals at week 11 postinfection also demonstrated increased frequencies of MAIT cells at the rectal mucosa following infection (Fig. 4E), suggesting that modulation of MAIT cell α4β7 expression is associated with trafficking of cells to the mucosa.

MAIT cells exhibit proliferative responses to acute infection

Concurrent with the increase in MAIT cell α4β7 expression at week 3 postinfection, the frequency of MAIT cells increased as a proportion of the total $CD8^+$ T cell population (Fig. 5A; median 1.06% at baseline, 1.72% at week 3). This increase in frequency was observed among animals infected with either SIV_{mac251} or $SHIV_{SF162P3}$ but not the CXCR4-tropic $SHIV_{mn229}$ virus (data not shown). A subset of samples was available to confirm whether the increase in MAIT cell frequency was due to cellular proliferation. MAIT cell Ki67 expression increased at week 3 postchallenge compared with baseline (median 5.9% $Ki67^+$ at baseline versus median 28.6% at week 3, $p = 0.004$; Fig. 5B, 5C) among five infected animals ($n = 3$ SIV_{mac251}, $n = 2$ $SHIV_{SF162P3}$). As expected, there was no appreciable change in the percentage of Ki67 staining MAIT cells in three contemporaneously studied animals completely protected from infection following challenge (Fig. 5B, 5C). The level of MAIT cell Ki67 expression at week 3 correlated with the fold-change in MAIT cell frequency between weeks 0 and 3 ($p = 0.011$, Fig. 5D), confirming that, rather than being rapidly depleted postinfection, MAIT cells proliferate and increase in frequency.

Early chronic SIV/SHIV infection does not result in MAIT cell depletion or loss of CCR6 expression

In humans, depletion of the peripheral MAIT cell population occurs as early as 2–3 wk post–HIV infection (46), with significant depletion during the first year of disease progression (14, 16) and concomitant loss of CCR6 expression (14). We did not, however, observe any consistent impact of SIV/SHIV infection on peripheral MAIT cell frequency out to a maximum of 81 wk postchallenge (Fig. 6A, 6B), as the transient increase in MAIT cell frequency observed at week 3 was not maintained over the course of infection. Similar patterns were observed regardless of whether MAIT cell frequency was presented as a proportion of $CD8^+$ T cells (Fig. 6B) or $CD3^+$ T cells (Supplemental Fig. 4C). When expressed as absolute cell counts per microliter, six out of seven SIV_{mac251}-infected animals showed little or no change in MAIT cell numbers, with only one animal exhibiting substantial depletion after 40 wk of chronic infection (Supplemental Fig. 4D, animal 9175). No $SHIV_{mn229}$-infected animals showed MAIT cell loss. Similarly, there was no overall pattern of rise or fall of MAIT cells in four animals infected with $SHIV_{SF162P3}$. Overall, based on 15 animals studied, we conclude that in three virus infection models studied (SIV and two SHIV models), infection had no consistent or appreciable impact on PTM MAIT cell frequency or absolute counts within the first year of infection.

Similarly, we found CCR6 surface expression on MAIT cells was consistent throughout infection. Only two of the fifteen animals studied exhibited loss in the frequency of CCR6 expression. One had an abnormally low percentage of CCR6 expressing MAIT cells at baseline (Fig. 6C, 6D); the other animal, 9175, was the same animal that exhibited substantial MAIT cell depletion (Fig. 6A). There were no unique aspects of viral load, CD4 loss, or other infections associated with the single case of MAIT cell loss and reduction of $CCR6^+$ MAIT cells.

MAIT cells become activated and lose Tbet expression during chronic infection

By 36 wk postchallenge, animals infected with SIV_{mac251} exhibited a significant increase in the percentage of $CD69^+$ MAIT cells (median 21% $CD69^+$) compared with baseline (median 8.8% $CD69^+$, $p = 0.008$; Fig. 7A, 7B). $SHIV_{mn229}$-infected animals exhibited a similar increase in MAIT cell activation by week 11 of infection (median

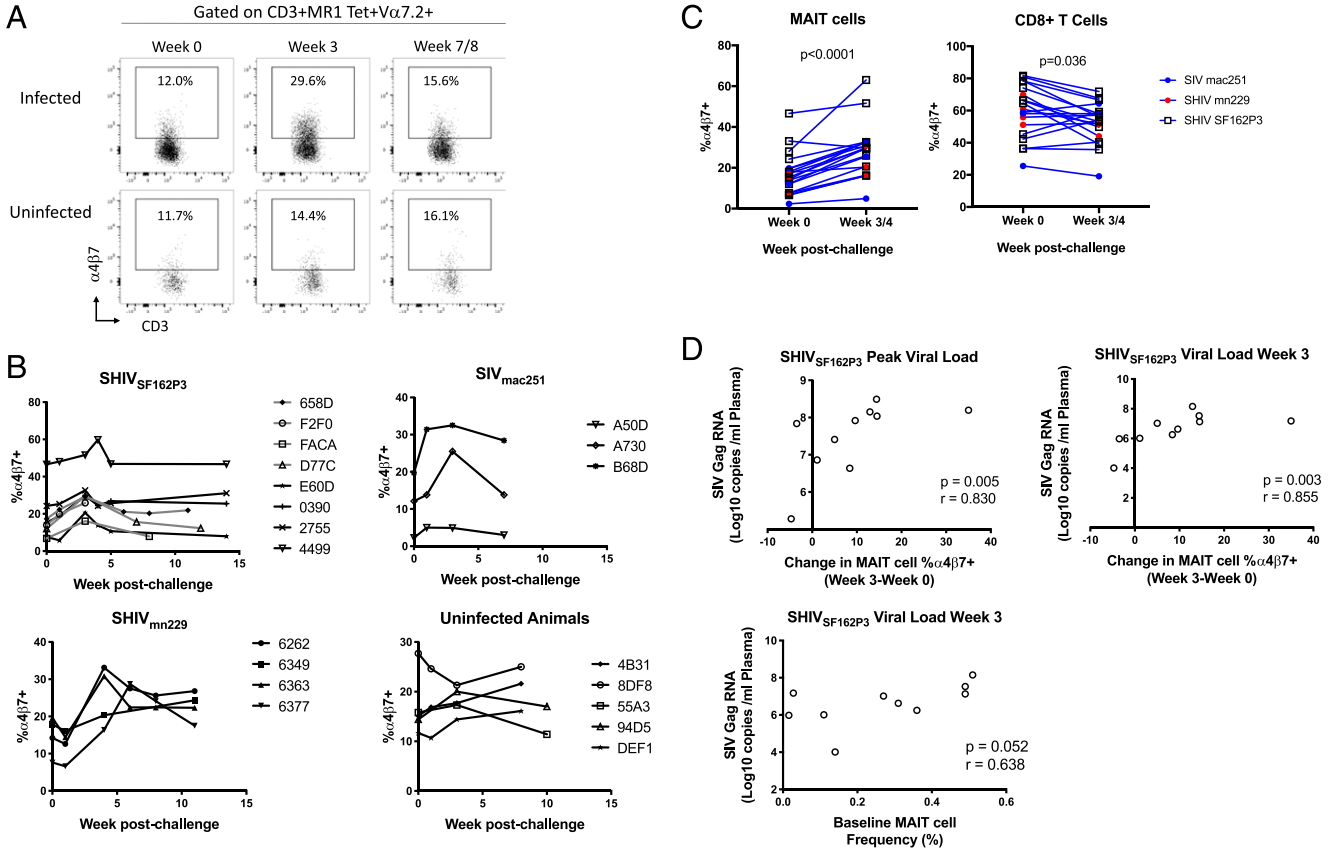

FIGURE 3. Acute SIV/SHIV infection induces MAIT cell α4β7 expression. (**A**) Representative staining of α4β7 surface expression on MAIT cells in one animal that became infected (weeks 0, 3, and 7 postchallenge) and one animal that remained uninfected (weeks 0, 3, and 8 postchallenge). (**B**) Quantification of MAIT cell α4β7 expression over time in animals exhibiting viremia at week 1 postchallenge or animals that remained uninfected following challenge. Among $SHIV_{SF162P3}$-infected animals, gray indicates animals challenged i.v. and black indicates intrarectal challenge. (**C**) Statistical analysis of MAIT cell or non-MAIT $CD8^+$ T cell α4β7 expression at baseline and week 3 postchallenge among animals infected with SIV_{mac251} ($n = 3$, blue circles), $SHIV_{mn229}$ ($n = 4$, red circles), and $SHIV_{SF162P3}$ ($n = 12$, open squares), compared with animals that were challenged but remained uninfected ($n = 5$). All infected animals shown exhibited detectible viremia by 1 wk postchallenge. Statistics assessed by Kruskal–Wallis test and Dunn multiple comparisons posttest. (**D**) Correlation between the change in MAIT cell α4β7 expression (week 3 minus week 0) or baseline MAIT cell frequency and peak viral load or viral load at week 3 postchallenge among all animals challenged intrarectally with $SHIV_{SF162P3}$ ($n = 10$). Statistics assessed by Spearman correlation.

11.5% $CD69^+$ at baseline versus 21.9% at week 11; Fig. 7A, 7B). This MAIT cell activation was associated with alterations in MAIT cell transcription factor expression, similar to previous observations in studies of chronic HIV infection (20). Whereas the predominant phenotype of PTM MAIT cells is $Tbet^{dim}Eomes^+$ (Fig. 7D), a significant loss of Tbet expression was observed by week 18–40 postchallenge in animals infected with either $SHIV_{SF162P3}$ or SIV_{mac251}, as well as by week 11 in animals infected with $SHIV_{mn229}$ (Fig. 7D–F). Some animals also exhibited a loss of Eomes expression during infection (data not shown), although changes in Eomes were not as consistent across animals and infecting viruses as the loss of Tbet expression.

Because a $Tbet^-Eomes^-$ MAIT cell phenotype is associated with poor IFN-$\gamma^+CD107a^+$ responses to stimulation in chronically HIV-infected individuals (20), we assessed MAIT cell function in response to 5-OP-RU stimulation (in the presence of IL-12 and IL-18). Among five animals for whom samples were available to match the Tbet expression data, there was no consistent decrease in MAIT cell response to stimulation (Fig. 7G). Interestingly, however, the only animal that exhibited reduced MAIT cell function following infection (F2F0) was also the only animal out of the five to exhibit a loss of MAIT cell Eomes expression (Fig. 7H) in addition to the reduction in Tbet expression.

MAIT cells are not substantially perturbed in tissues during SIV/SHIV infection

Despite the maintenance of peripheral MAIT cell frequency, changes in MAIT cell recruitment to and proliferation in mucosal and lymphoid tissues may not be reflected in PBMC samples. Although there were no significant differences in the ratio of MAIT cell frequency between PBMC and liver or PBMC and spleen between uninfected and infected animals, the ratios tended to be lower in infected animals (Fig. 8A). In the peripheral inguinal LN samples, the inguinal LN/PBMC MAIT cell frequency ratio was significantly lower in SHIV/SIV infected animals than uninfected controls ($p = 0.0095$). In contrast, no significant discrepancy was observed in MLN samples. In contrast to the LN, BAL MAIT cells increased in frequency following $SHIV_{SF162P3}$ infection (Fig. 8B, 8C). The enrichment of MAIT cell frequency in the lung was greater among infected animals at week 11 compared with naive controls ($p = 0.031$, Fig. 8D), suggesting preferential MAIT cell recruitment to, or local proliferation in, the lung during SHIV infection.

MAIT cell CCR6 expression was modified in some tissues, including the liver (Fig. 8E), likely reflecting chemokine receptor internalization upon binding to CCL20, which is constitutively expressed in the liver (47), but no SIV-specific changes were observed. The percentage of tissue and LN-derived MAIT cells that expressed the activation/tissue retention marker CD69 was

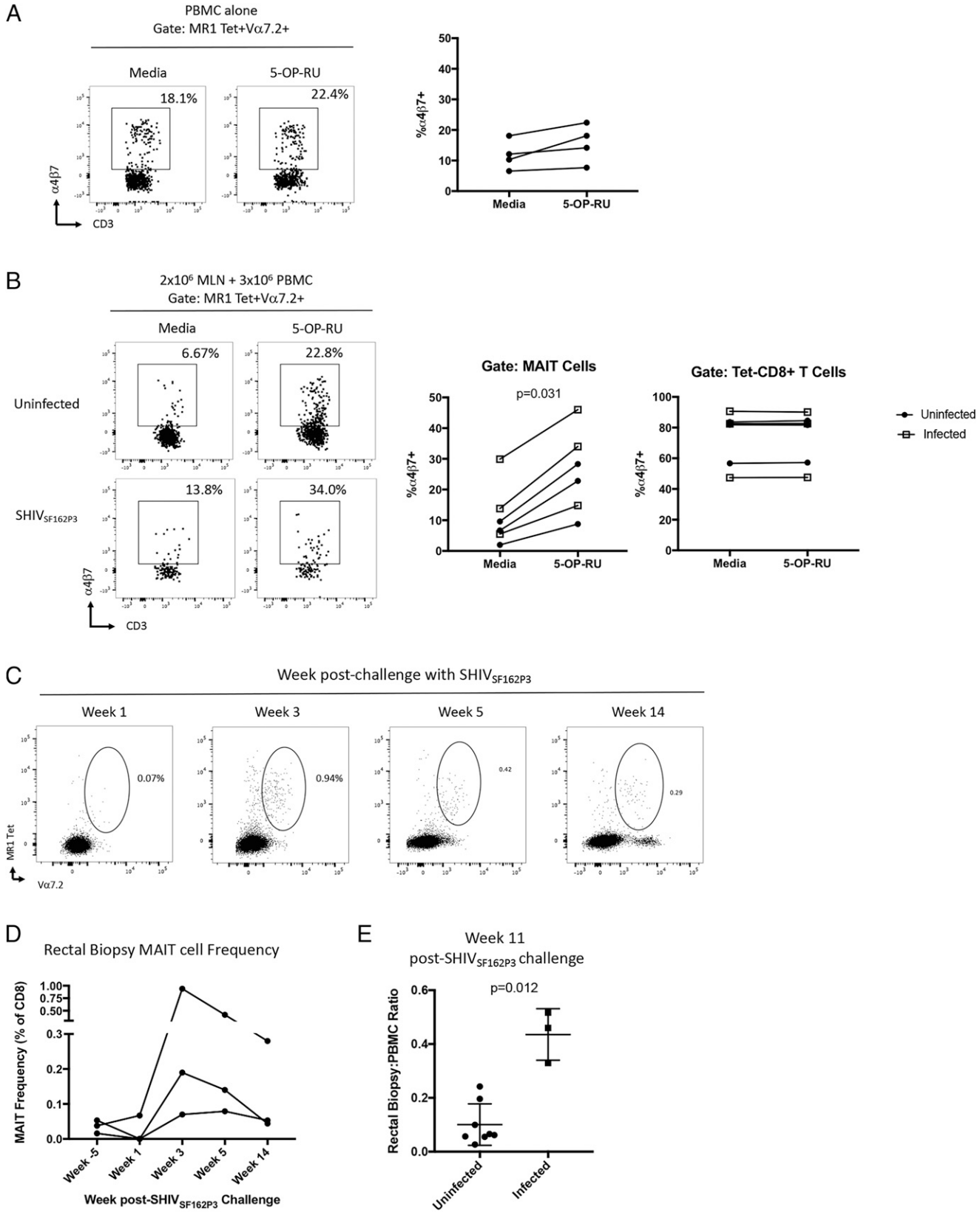

FIGURE 4. MAIT cell α4β7 expression is induced by Ag and associated with MAIT cell recruitment to the rectum. (**A**) Freshly isolated PBMC were stimulated with 10 nM 5-OP-RU and cultured in the presence of human rIL-2 for 3 d. Plots show representative α4β7 expression on gated MAIT cells in the media control and 5-OP-RU–stimulated conditions. Graph indicates quantification of α4β7 expression among four individual animals. (**B**) A total of 2×10^6 MLN cells were cultured with 3×10^6 autologous PBMC for 3 d in the presence or absence of 10 nM 5-OP-RU. Plots show MAIT cell α4β7 expression at day 3 in media (control) or 5-OP-RU–stimulated cocultures for one uninfected and one $SHIV_{SF162P3}$ animal. Statistical assessment of changes in the frequency of α4β7 expressing MAIT cells or non-MAIT $CD8^+$ T cells between control and 5-OP-RU–stimulated cultures was assessed by Wilcoxon test. (**C**) Identification of rectal MAIT cells in a single animal at weeks 1, 3, 5, and 14 after challenge with $SHIV_{SF162P3}$. (**D**) Comparison of MAIT cell frequency (as a proportion of $CD8^+$ T cells) in rectal biopsy samples of three animals at weeks −5, 1, 3, 5, and 14 postchallenge. (**E**) Comparison of MAIT cell frequency in rectal biopsy samples relative to PBMC among eight uninfected and three $SHIV_{SF162P3}$-infected (week 11) animals at necropsy.

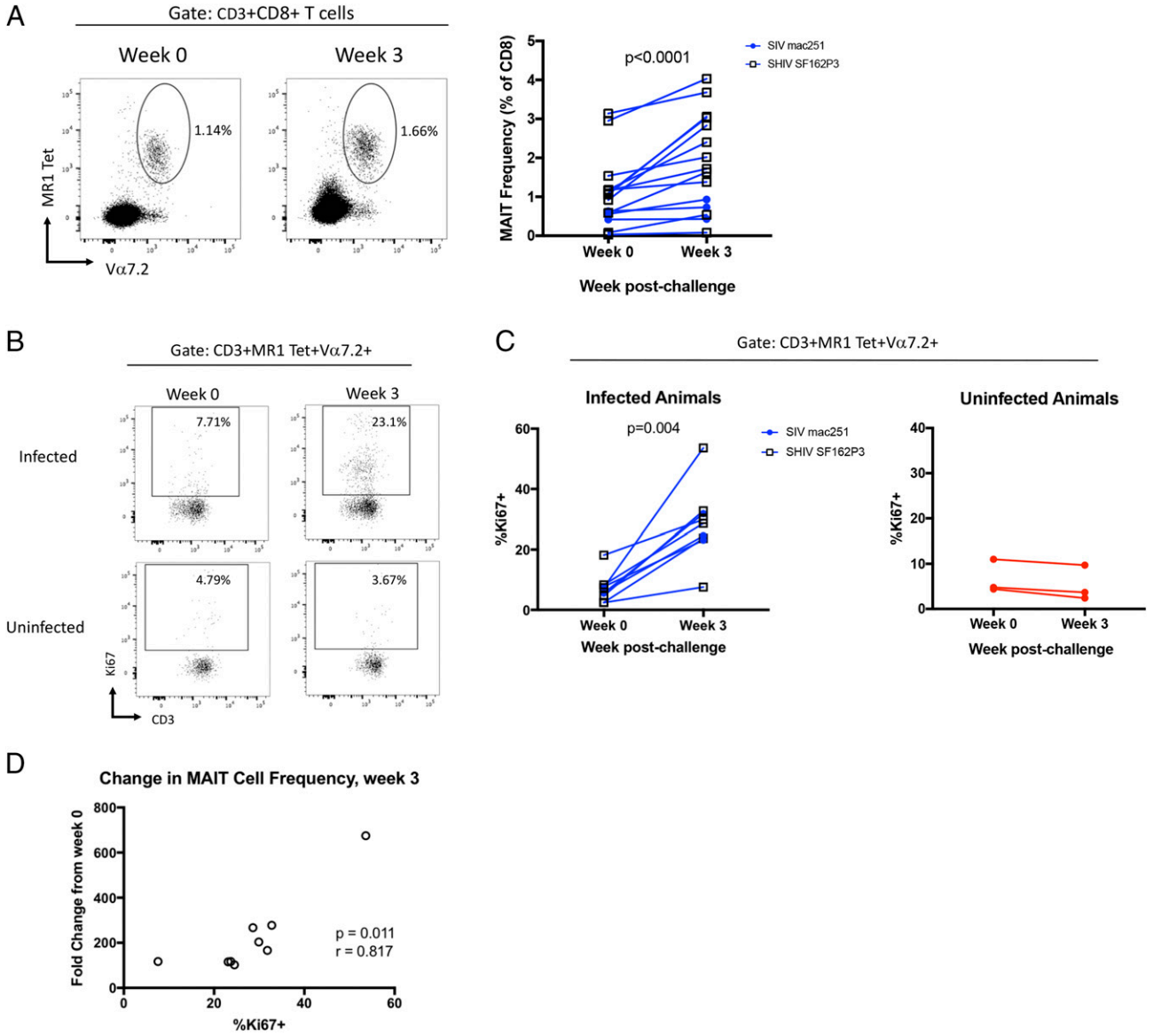

FIGURE 5. Acute SIV/SHIV infection induces proliferation of MAIT cells. (**A**) Representative staining and quantification of MAIT cell frequency as a percentage of $CD8^+$ T cells at weeks 0 and 3 postinfection (n = 3 SIV_{mac251} and n = 12 $SHIV_{SP162P3}$). Statistics assessed by Wilcoxon test. (**B**) Representative intracellular Ki67 expression at weeks 0 and 3 in MAIT cells of one animal that became infected and one animal that remained uninfected after viral challenge. (**C**) Quantification of MAIT cell Ki67 expression among animals infected with SIV_{mac251} (n = 3) and $SHIV_{SF162P3}$ (n = 2) at weeks 0 and 3 compared with uninfected animals. (**D**) Spearman correlation between the proportion of $Ki67^+$ MAIT cells and the fold change in MAIT cell frequency between weeks 0 and 3 postinfection.

elevated compared with PBMCs (Fig. 8F), particularly in the MLN, liver and thymus, but the percentage of CD69 expression on MLN or liver MAIT cells was comparable between both groups of animals (Fig. 8F).

Discussion

This study provides the first insights, to our knowledge, into the longitudinal impact of three distinct SIV/SHIV viral infections on peripheral and tissue-derived PTM MAIT cells. These detailed analyses were made possible through constructing a PTM MR1 tetramer homogeneously loaded with the potent MAIT cell Ag 5-OP-RU. Consistent with MAIT cells previously identified in humans, we showed that the PTM MR1–5-OP-RU tetramer specifically identified a population of T cells that was $V\alpha7.2^+$, uniformly $PLZF^+$, $CCR6^+$, and $IL\text{-}18Ra^+$ and of which the majority displayed a $Tbet^{dim}Eomes^+$ phenotype. This PTM MR1 tetramer reagent should be useful to the field of macaque MAIT cell biology, because we find it improves upon PTM MAIT cell identification compared with human MR1–5-OP-RU–loaded tetramers.

The suboptimal tetramer cross-reactivity is somewhat surprising, because human and macaque MR1 only differ in 10 aa in the α1 and α2 domains, and the 26.5 and 8F2.F9 mAbs bind to both to a similar extent in ELISA. An analysis of all currently available crystal structures of ternary complexes with human MR1–5-OP-RU and human MAIT TCRs (Supplemental Fig. 2) indicates that all MR1 residues contacted in hydrogen bonds (there are no salt bridges) are conserved between human and macaque MR1. Furthermore, Vinton et al. (21) found that some public MAIT TCR α-chains in rhesus macaques are also found in humans, so it is possible that there is some overlap in the macaque and human MAIT cell repertoire. As previously noted by Greene et al. (22) based on analysis of a human MAIT TCR bound to bovine MR1, three of the residues that differ between human and macaque MR1 (M72, L151, E159) are, however, contacted in Van der Waals

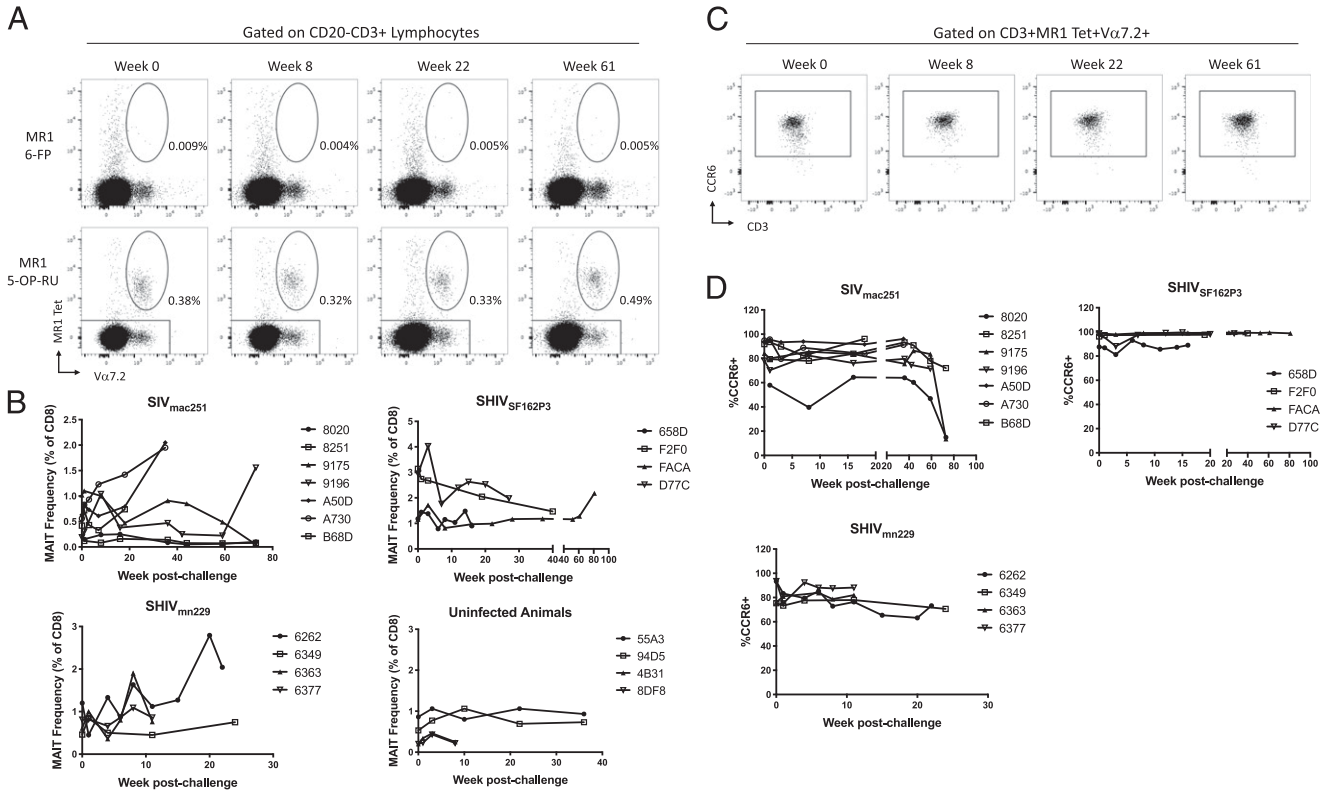

FIGURE 6. Chronic SIV/SHIV infection does not result in peripheral MAIT cell depletion. (**A**) Representative staining of MR1–6-FP or MR1–5-OP-RU tetramer and Vα7.2 in animal FACA challenged with $SHIV_{SF162P3}$ at weeks 0, 8, 22, and 61 postchallenge. (**B**) MAIT cell frequency as a proportion of $CD8^+$ T cells in animals infected with $SHIV_{SF162P3}$ ($n = 4$), SIV_{mac251} ($n = 4$ i.v. challenge, $n = 3$ intrarectal challenge), or $SHIV_{mn229}$ ($n = 4$). Animals protected from infection ($n = 4$) are shown as a control. (**C**) Representative staining of MAIT cell CCR6 expression in animal FACA at weeks 0, 8, 22, and 61 postchallenge. (**D**) MAIT cell CCR6 expression over time in animals challenged with $SHIV_{SF162P3}$ ($n = 4$), SIV_{mac251} ($n = 7$), or $SHIV_{mn229}$ ($n = 4$).

bonds by the TCR, and the same is true in available ternary complexes with human MR1–5-OP-RU and human MAIT TCRs (except for Protein Data Bank identifier 4PJ9 where M72 is not a Van der Waals contact). At the same time, differing residues might have indirect effects on recognition of conserved residues of MR1. This includes MR1 residues E159K, a charge reversal, and L151R, a change from a nonpolar to a charged residue. These two residues are in close spatial proximity to MR1 residues N155 and E160 and residues H148, Y152, N155, respectively, which are conserved between human and macaque MR1 and which are contacted in hydrogen bonds by TCRs in human crystal structures. Thus, respective MAIT TCR repertoires of the two species might be fine-tuned to accommodate for these differences, with changes potentially focused in the MAIT TCRβ-chain. As a result, whereas MR1 is highly conserved among species including human and macaque, species-specific differences in the MAIT TCR–MR1 axis exist and future crystal structures might shed light on the relevant molecular details.

Our analysis of PTM MAIT cells provides a comprehensive phenotypic analysis of NHP-derived MAIT cells and demonstrates the large degree of phenotypic similarity between macaque and human MAIT cells. Surprisingly, substantial differences in α4β7 and PD-1 expression were observed between PTM and human MAIT cells. Studies of T cell α4β7 acquisition in humans, mice, and NHPs suggest that APCs in the MLN and gut have the unique capacity to induce α4β7 expression following Ag exposure in the context of retinoic acid (38, 43–45). The idea that MAIT cell exposure to Ag may differ between macaques and humans is consistent with data generated by Greene et al. (22) which show differences in MAIT cell memory status between humans and NHP, and throughout distinct NHP tissues.

This is the first study, to our knowledge, to provide a longitudinal analysis of MAIT cell dynamics immediately following SIV/SHIV infection. MAIT cells appear to respond to early viral replication through the robust upregulation of the integrin and gp120-binding protein α4β7, regardless of viral tropism or route of infection. The importance of α4β7 expression in human and NHP susceptibility to HIV/SIV has been emphasized in recent translational studies using anti-α4β7 Abs (48–50), although to our knowledge, no publications to date have assessed MAIT cell trafficking during α4β7 blockade or therapeutic intervention in NHPs. It is likely that MAIT cell α4β7 upregulation at week 3 after SIV infection reflects exposure to Ag caused by gut barrier disruption and microbial translocation. Furthermore, our analysis of rectal biopsies suggests that MAIT cells are indeed recruited to the gut mucosa following SIV/SHIV infection. This timing is consistent with the results of detailed studies of microbial translocation in macaques; increases in the number of bacterial genera detected in plasma peaks one week postinfection, whereas elevated plasma sCD14 is detected at week three (51).

Given the substantial similarities between human and PTM MAIT cells, it was surprising that we found no evidence of MAIT cell depletion during early SIV/SHIV infection. Although peripheral MAIT cell depletion is most commonly reported during chronic HIV infection or antiretroviral therapy (16, 17), several human cohort studies report significantly reduced MAIT cell frequencies in individuals at ∼3–12 mo postinfection (14, 16), and one study demonstrated MAIT cell depletion as early as 2–3 wk following infection (46). Although the data from Vinton et al. (21) suggest that chronic SIV infection and substantial $CD4^+$ T cell depletion are associated with low MAIT cell frequencies, it is

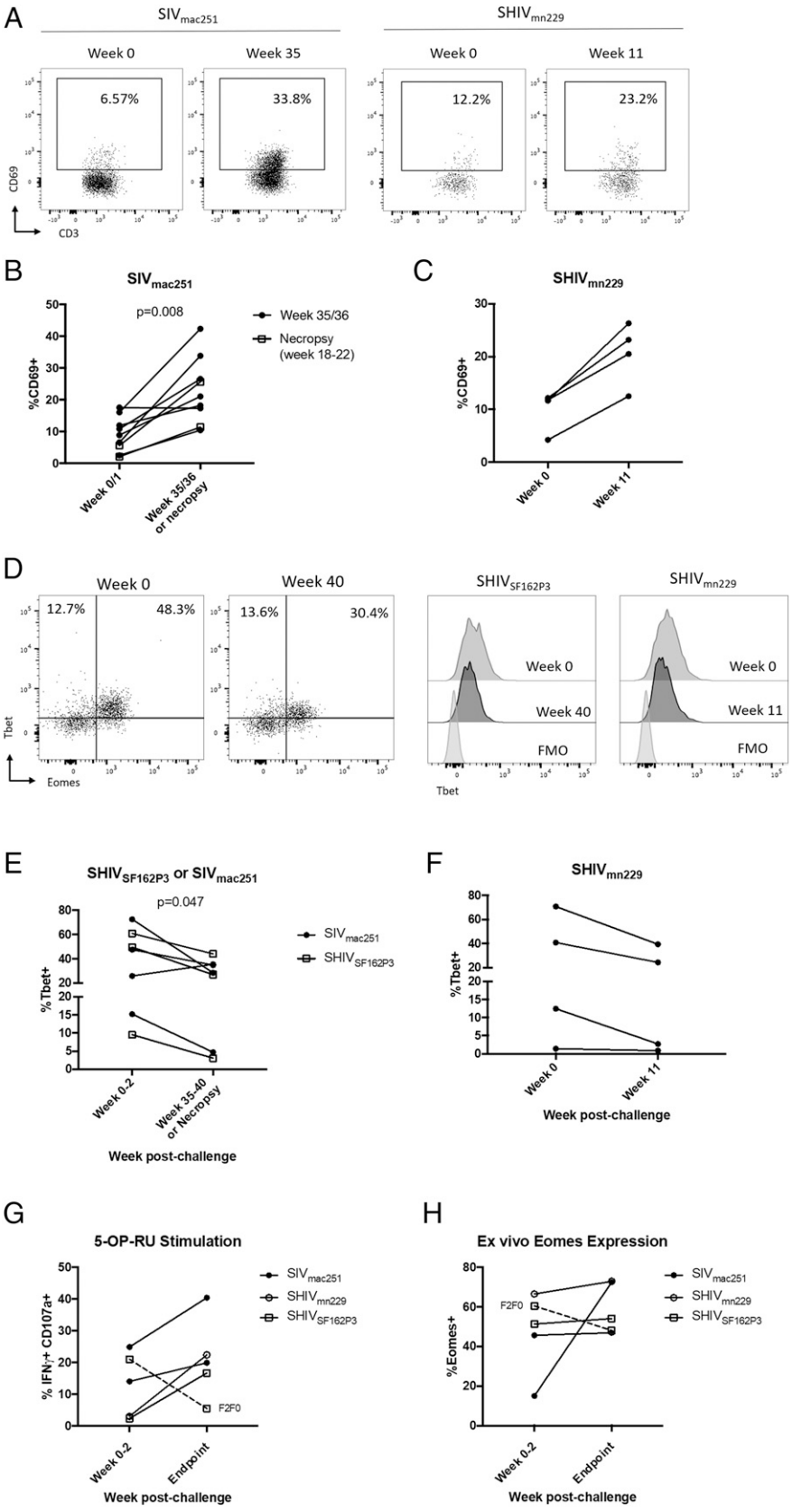

FIGURE 7. MAIT cells are activated and lose Tbet expression during chronic SIV/SHIV infection. (**A**) Representative CD69 expression on MAIT cells during CCR5-tropic (SIV_{mac251}) or CXCR4-tropic ($SHIV_{mn229}$) infection at week 35 for less pathogenic infections, or week 11 for more pathogenic infections. (**B**) Statistical analysis of MAIT cell CD69 expression at week 35/36 postchallenge or time of necropsy for animals infected with SIV_{mac251}. Statistics assessed by Wilcoxon test. (**C**) Analysis of four animals infected with $SHIV_{mn229}$ revealed similar increases in frequency of CD69 expressing MAIT cells at 11 wk postchallenge compared with baseline. (**D**) Representative staining of MAIT cell Tbet and Eomes coexpression (dot plot) or total Tbet expression (histograms) at week 0 and week 40 of an animal infected with $SHIV_{SF162P3}$ and week 0 and week 11 of an animal infected with $SHIV_{mn229}$. (**E**) Statistical assessment of the frequency of $Tbet^+$ MAIT cells in animals infected with CCR5-tropic virus ($SHIV_{SF162P3}$ or SIV_{mac251}) at week 35–40 or necropsy compared with baseline. Only some animals had samples available for transcriptional analysis. Statistics assessed by Wilcoxon test. (**F**) A similar loss of the frequency of Tbet-expressing MAIT cells at week 11 postchallenge was observed in three out of four $SHIV_{mn229}$-infected animals, with the exception of one animal that exhibited negligible loss in the frequency of Tbet expression at baseline. (**G**) Samples from five animals in (E) and (F) were stimulated with 5-OP-RU for 16 h in the presence of macaque rIL-12 and rIL-18. Samples were obtained from the same baseline or end point date as the as samples used for Tbet analysis (end point was week 35–40 or necropsy for SIV_{mac251}/$SHIV_{SF162P3}$–infected animals, or week 11 for $SHIV_{mn229}$-infected animals). Data are presented as the proportion of IFN-$\gamma^+CD107a^+$ MAIT cells after background subtraction using a medium + IL-12 + IL-18 control. Animal F2F0 is indicated with a dashed line. (**H**) MAIT cell Eomes expression among animals and timepoints matched to (G).

clear from our data that early chronic infection with either CCR5- or CXCR4-tropic viruses does not result in substantial MAIT cell loss in PTM. Given the substantial variability in baseline MAIT cell frequency between macaques in our studies and in human cohorts (14, 16), additional longitudinal studies may be required to confirm the impact of highly progressive SIV infection on MAIT cell frequency.

The lack of MAIT cell α4β7 expression and population of the rectal mucosa provides several plausible explanations for the differential impact of early SIV and HIV on MAIT cell

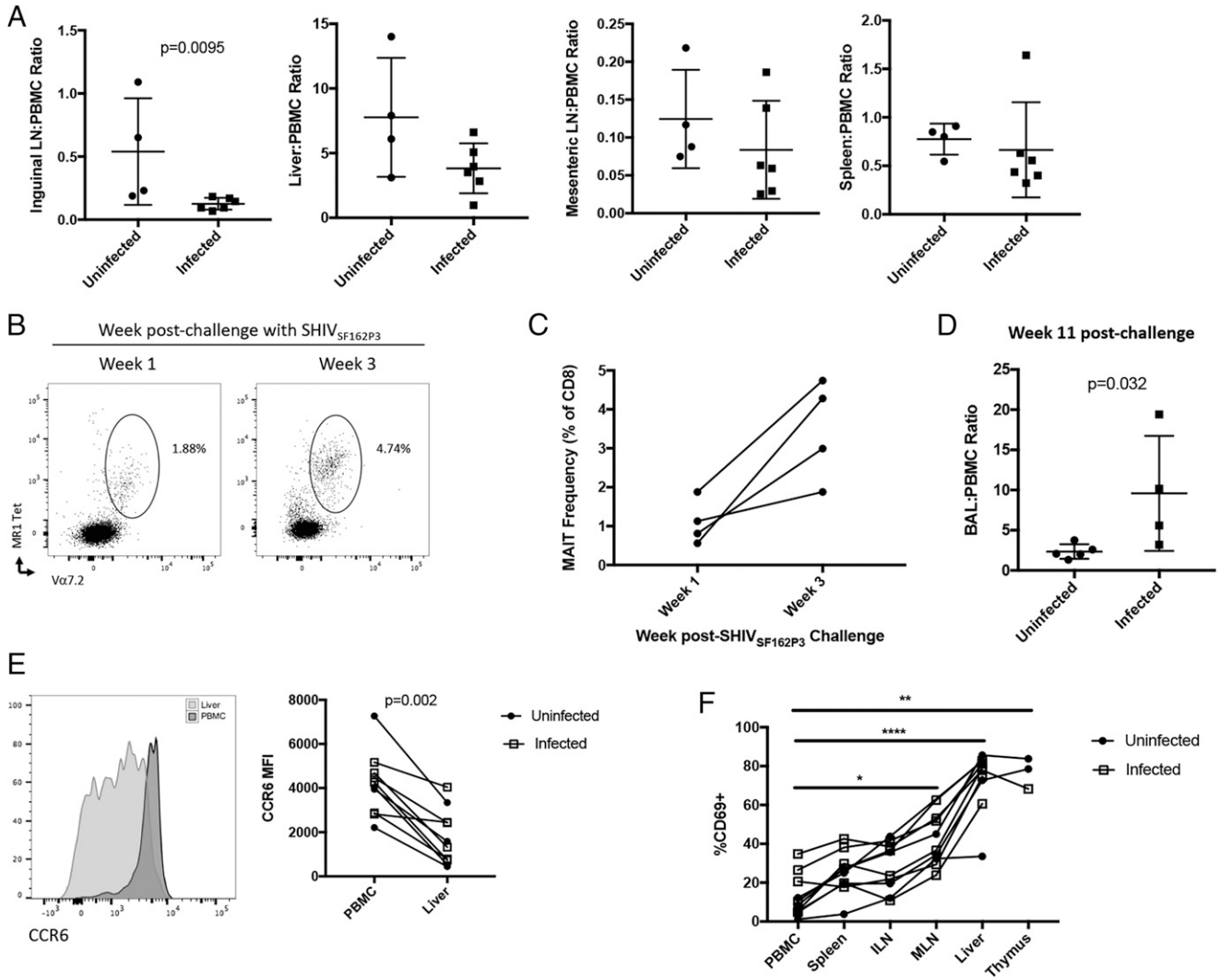

FIGURE 8. MAIT cell frequency in tissues of naive and SIV/SHIV–infected macaques. (**A**) Ratio of MAIT cell frequency in tissue samples versus PBMC for uninfected and SIV/SHIV$^+$ animals. Statistics assessed by Mann–Whitney *U* test. (**B**) Identification of BAL MAIT cells in a single animal at week 1 and week 3 after challenge with SHIV$_{SF162P3}$. (**C**) Comparison of MAIT cell frequency (as a proportion of CD8$^+$ T cells) in BAL samples of four animals at weeks 1 and 3 postchallenge. (**D**) Comparison of MAIT cell frequency in BAL relative to PBMC among five uninfected and four SHIV$_{SF162P3}$-infected (week 11) animals at necropsy. (**E**) Representative histogram and statistical analysis of MAIT cell CCR6 mean fluorescence intensity in PBMC versus liver samples, $n = 10$ animals; 6 infected (open squares) and 4 uninfected (closed circles). (**F**) Quantification of the frequency of MAIT cells expressing CD69 among all six tissues analyzed. $n = 10$ animals; 6 infected (open squares) and 4 uninfected (closed circles), except for thymus samples in which only two infected and one uninfected animal exhibited sufficient MAIT events for analysis. Statistics assessed by Kruskal–Wallis test, with Dunn multiple comparisons posttest comparing all tissues to the PBMC control. $*p < 0.05$, $**p < 0.01$, $****p < 0.0001$.

frequency in PTMs. First, it is tempting to speculate that PTM MAIT cells may be partially protected from gp120-induced cell death by their low level of α4β7 expression. Li and Pauza (52) demonstrated that CD4$^-$ Vδ2$^+$ T cells are likely depleted in the peripheral blood of HIV-infected individuals because of gp120-mediated cross-linking of α4β7 and CCR5 surface proteins and subsequent caspase activation. Human MAIT cells share this uniform CD4$^-$CCR5^{hi}α4β7$^+$ phenotype and thus might be susceptible to the same apoptosis program, whereas macaque MAIT cells express significantly less α4β7 and therefore are unlikely to undergo a similar degree of apoptosis by this mechanism. Second, reduced MAIT cell recruitment to the gut in macaques compared with humans is likely to result in less overall exposure to translocated microbial products, and lower levels of activation-induced cell death, thereby preserving MAIT cell frequency in the periphery. The striking relationship between low MAIT cell α4β7 expression, a lack of MAIT cell enrichment at the gut, and the lack of MAIT cell depletion during SIV infection suggests that immunotherapeutic strategies to modify MAIT cell trafficking in humans might help to preserve MAIT cell numbers and boost immunity to bacterial coinfections such as TB.

After~9 mo of infection, the MAIT cell population exhibited activation and a loss of Tbet expression. Despite this phenotype, MAIT cell function appeared to be preserved, except for one animal who exhibited a loss of both Tbet and Eomes expression in the MAIT cell population. This data are broadly consistent with that of a human cohort studied between 1 mo and 1 y postinfection, in which MAIT cell function was unperturbed compared with healthy controls (14). It also suggests the possibility that, as in humans, an accumulation of Tbet$^-$Eomes$^-$ MAIT cells is associated with loss of MAIT cell responses to stimulation (20). Unfortunately, the high baseline expression of PD-1 on healthy PTM macaque MAITs made it difficult to assess immune exhaustion through further increases in MAIT cell PD-1 following SIV/SHIV

infection. In the absence of data regarding MAIT cell phenotype in other NHP species, it is unclear as to whether PD-1 expression by PTM MAIT cells is unique. It is known that healthy PTMs exhibit greater gut permeability than rhesus macaques (24), making it possible that constitutive low-level immune stimulation may result in the high levels of PD-1 expression we observed. Future comparative studies of NHP MAIT phenotypes will be informative in assessing the relationship between gut permeability and MAIT cell PD-1 and/or α4β7 expression.

Acknowledgments

We thank T. Hansen (University of Washington) and W.J. Yankelevich (U.S. Food and Drug Administration) for the gifts of the 26.5 and 8F2.F9 hybridomas. We also thank the staff of the Doherty Institute ImmunoID Flow Core and animal care technicians at the Commonwealth Scientific and Industrial Research Organization animal facility for contributions to the study.

Disclosures

The authors have no financial conflicts of interest.

References

1. Kjer-Nielsen, L., O. Patel, A. J. Corbett, J. Le Nours, B. Meehan, L. Liu, M. Bhati, Z. Chen, L. Kostenko, R. Reantragoon, et al. 2012. MR1 presents microbial vitamin B metabolites to MAIT cells. *Nature* 491: 717–723.
2. Corbett, A. J., S. B. Eckle, R. W. Birkinshaw, L. Liu, O. Patel, J. Mahony, Z. Chen, R. Reantragoon, B. Meehan, H. Cao, et al. 2014. T-cell activation by transitory neo-antigens derived from distinct microbial pathways. *Nature* 509: 361–365.
3. Ussher, J. E., M. Bilton, E. Attwod, J. Shadwell, R. Richardson, C. de Lara, E. Mettke, A. Kurioka, T. H. Hansen, P. Klenerman, and C. B. Willberg. 2014. CD161++ CD8+ T cells, including the MAIT cell subset, are specifically activated by IL-12+IL-18 in a TCR-independent manner. *Eur. J. Immunol.* 44: 195–203.
4. van Wilgenburg, B., I. Scherwitzl, E. C. Hutchinson, T. Leng, A. Kurioka, C. Kulicke, C. de Lara, S. Cole, S. Vasanawathana, W. Limpitikul, et al; STOP-HCV Consortium. 2016. MAIT cells are activated during human viral infections. *Nat. Commun.* 7: 11653.
5. Wong, E. B., T. Ndung'u, and V. O. Kasprowicz. 2017. The role of mucosal-associated invariant T cells in infectious diseases. *Immunology* 150: 45–54.
6. Meierovics, A., W. J. Yankelevich, and S. C. Cowley. 2013. MAIT cells are critical for optimal mucosal immune responses during in vivo pulmonary bacterial infection. *Proc. Natl. Acad. Sci. USA* 110: E3119–E3128.
7. Georgel, P., M. Radosavljevic, C. Macquin, and S. Bahram. 2011. The non-conventional MHC class I MR1 molecule controls infection by *Klebsiella pneumoniae* in mice. *Mol. Immunol.* 48: 769–775.
8. Wang, H., C. D'Souza, X. Y. Lim, L. Kostenko, T. J. Pediongco, S. B. G. Eckle, B. S. Meehan, M. Shi, N. Wang, S. Li, et al. 2018. MAIT cells protect against pulmonary *Legionella* longbeachae infection. *Nat. Commun.* 9: 3350.
9. Loh, L., Z. Wang, S. Sant, M. Koutsakos, S. Jegaskanda, A. J. Corbett, L. Liu, D. P. Fairlie, J. Crowe, J. Rossjohn, et al. 2016. Human mucosal-associated invariant T cells contribute to antiviral influenza immunity via IL-18-dependent activation. *Proc. Natl. Acad. Sci. USA* 113: 10133–10138.
10. Gold, M. C., R. J. Napier, and D. M. Lewinsohn. 2015. MR1-restricted mucosal associated invariant T (MAIT) cells in the immune response to *Mycobacterium tuberculosis. Immunol. Rev.* 264: 154–166.
11. Chua, W. J., S. M. Truscott, C. S. Eickhoff, A. Blazevic, D. F. Hoft, and T. H. Hansen. 2012. Polyclonal mucosa-associated invariant T cells have unique innate functions in bacterial infection. *Infect. Immun.* 80: 3256–3267.
12. Salou, M., K. Franciszkiewicz, and O. Lantz. 2017. MAIT cells in infectious diseases. *Curr. Opin. Immunol.* 48: 7–14.
13. Saeidi, A., R. Ellegård, Y. K. Yong, H. Y. Tan, V. Velu, J. E. Ussher, M. Larsson, and E. M. Shankar. 2016. Functional role of mucosal-associated invariant T cells in HIV infection. *J. Leukoc. Biol.* 100: 305–314.
14. Fernandez, C. S., T. Amarasena, A. D. Kelleher, J. Rossjohn, J. McCluskey, D. I. Godfrey, and S. J. Kent. 2015. MAIT cells are depleted early but retain functional cytokine expression in HIV infection. *Immunol. Cell Biol.* 93: 177–188.
15. Saeidi, A., V. L. Tien Tien, R. Al-Batran, H. A. Al-Darraji, H. Y. Tan, Y. K. Yong, S. Ponnampalavanar, M. Barathan, D. V. Rukumani, A. W. Ansari, et al. 2015. Attrition of TCR Vα7.2+ CD161++ MAIT cells in HIV-tuberculosis co-infection is associated with elevated levels of PD-1 expression. *PLoS One* 10: e0124659.
16. Cosgrove, C., J. E. Ussher, A. Rauch, K. Gärtner, A. Kurioka, M. H. Hühn, K. Adelmann, Y. H. Kang, J. R. Fergusson, P. Simmonds, et al. 2013. Early and nonreversible decrease of CD161++ /MAIT cells in HIV infection. *Blood* 121: 951–961.
17. Leeansyah, E., A. Ganesh, M. F. Quigley, A. Sönnerborg, J. Andersson, P. W. Hunt, M. Somsouk, S. G. Deeks, J. N. Martin, M. Moll, et al. 2013. Activation, exhaustion, and persistent decline of the antimicrobial MR1-restricted MAIT-cell population in chronic HIV-1 infection. *Blood* 121: 1124–1135.
18. Dillon, S. M., D. N. Frank, and C. C. Wilson. 2016. The gut microbiome and HIV-1 pathogenesis: a two-way street. *AIDS* 30: 2737–2751.
19. Brenchley, J. M., D. A. Price, T. W. Schacker, T. E. Asher, G. Silvestri, S. Rao, Z. Kazzaz, E. Bornstein, O. Lambotte, D. Altmann, et al. 2006. Microbial translocation is a cause of systemic immune activation in chronic HIV infection. *Nat. Med.* 12: 1365–1371.
20. Leeansyah, E., J. Svärd, J. Dias, M. Buggert, J. Nyström, M. F. Quigley, M. Moll, A. Sönnerborg, P. Nowak, and J. K. Sandberg. 2015. Arming of MAIT cell cytolytic antimicrobial activity is induced by IL-7 and defective in HIV-1 infection. *PLoS Pathog.* 11: e1005072.
21. Vinton, C., F. Wu, J. Rossjohn, K. Matsuda, J. McCluskey, V. Hirsch, D. A. Price, and J. M. Brenchley. 2016. Mucosa-associated invariant T cells are systemically depleted in simian immunodeficiency virus-infected rhesus macaques. *J. Virol.* 90: 4520–4529.
22. Greene, J. M., P. Dash, S. Roy, C. McMurtrey, W. Awad, J. S. Reed, K. B. Hammond, S. Abdulhaqq, H. L. Wu, B. J. Burwitz, et al. 2016. MR1-restricted mucosal-associated invariant T (MAIT) cells respond to mycobacterial vaccination and infection in nonhuman primates. *Mucosal Immunol.* 10: 802–813.
23. Mak, J. Y., W. Xu, R. C. Reid, A. J. Corbett, B. S. Meehan, H. Wang, Z. Chen, J. Rossjohn, J. McCluskey, L. Liu, and D. P. Fairlie. 2017. Stabilizing short-lived Schiff base derivatives of 5-aminouracils that activate mucosal-associated invariant T cells. *Nat. Commun.* 8: 14599.
24. Klatt, N. R., L. D. Harris, C. L. Vinton, H. Sung, J. A. Briant, B. Tabb, D. Morcock, J. W. McGinty, J. D. Lifson, B. A. Lafont, et al. 2010. Compromised gastrointestinal integrity in pigtail macaques is associated with increased microbial translocation, immune activation, and IL-17 production in the absence of SIV infection. *Mucosal Immunol.* 3: 387–398.
25. De Rose, R., C. J. Batten, M. Z. Smith, C. S. Fernandez, V. Peut, S. Thomson, I. A. Ramshaw, B. E. Coupar, D. B. Boyle, V. Venturi, et al. 2007. Comparative efficacy of subtype AE simian-human immunodeficiency virus priming and boosting vaccines in pigtail macaques. *J. Virol.* 81: 292–300.
26. De Rose, R., C. S. Fernandez, M. Z. Smith, C. J. Batten, S. Alcântara, V. Peut, E. Rollman, L. Loh, R. D. Mason, K. Wilson, et al. 2008. Control of viremia and prevention of AIDS following immunotherapy of SIV-infected macaques with peptide-pulsed blood. *PLoS Pathog.* 4: e1000055.
27. Parsons, M. S., S. B. Lloyd, W. S. Lee, A. B. Kristensen, T. Amarasena, R. J. Center, B. F. Keele, J. D. Lifson, C. C. LaBranche, D. Montefiori, et al. 2017. Partial efficacy of a broadly neutralizing antibody against cell-associated SHIV infection. *Sci. Transl. Med.* 9: eaaf1483.
28. Reantragoon, R., A. J. Corbett, I. G. Sakala, N. A. Gherardin, J. B. Furness, Z. Chen, S. B. Eckle, A. P. Uldrich, R. W. Birkinshaw, O. Patel, et al. 2013. Antigen-loaded MR1 tetramers define T cell receptor heterogeneity in mucosal-associated invariant T cells. *J. Exp. Med.* 210: 2305–2320.
29. Huang, S., S. Gilfillan, M. Cella, M. J. Miley, O. Lantz, L. Lybarger, D. H. Fremont, and T. H. Hansen. 2005. Evidence for MR1 antigen presentation to mucosal-associated invariant T cells. *J. Biol. Chem.* 280: 21183–21193.
30. Chua, W. J., S. Kim, N. Myers, S. Huang, L. Yu, D. H. Fremont, M. S. Diamond, and T. H. Hansen. 2011. Endogenous MHC-related protein 1 is transiently expressed on the plasma membrane in a conformation that activates mucosal-associated invariant T cells. *J. Immunol.* 186: 4744–4750.
31. Kostenko, L., L. Kjer-Nielsen, I. Nicholson, F. Hudson, A. Lucas, B. Foley, K. Chen, K. Lynch, J. Nguyen, A. H. Wu, et al. 2011. Rapid screening for the detection of HLA-B57 and HLA-B58 in prevention of drug hypersensitivity. *Tissue Antigens* 78: 11–20.
32. McWilliam, H. E., S. B. Eckle, A. Theodossis, L. Liu, Z. Chen, J. M. Wubben, D. P. Fairlie, R. A. Strugnell, J. D. Mintern, J. McCluskey, et al. 2016. The intracellular pathway for the presentation of vitamin B-related antigens by the antigen-presenting molecule MR1. *Nat. Immunol.* 17: 531–537.
33. Meermeier, E. W., B. F. Laugel, A. K. Sewell, A. J. Corbett, J. Rossjohn, J. McCluskey, M. J. Harriff, T. Franks, M. C. Gold, and D. M. Lewinsohn. 2016. Human TRAV1-2-negative MR1-restricted T cells detect *S. pyogenes* and alternatives to MAIT riboflavin-based antigens. *Nat. Commun.* 7: 12506.
34. Gherardin, N. A., A. N. Keller, R. E. Woolley, J. Le Nours, D. S. Ritchie, P. J. Neeson, R. W. Birkinshaw, S. B. G. Eckle, J. N. Waddington, L. Liu, et al. 2016. Diversity of T cells restricted by the MHC class I-related molecule MR1 facilitates differential antigen recognition. *Immunity* 44: 32–45.
35. Gherardin, N. A., M. N. Souter, H. F. Koay, K. M. Mangas, T. Seemann, T. P. Stinear, S. B. Eckle, S. P. Berzins, Y. d'Udekem, I. E. Konstantinov, et al. 2018. Human blood MAIT cell subsets defined using MR1 tetramers. *Immunol. Cell Biol.* 96: 507–525.
36. Dusseaux, M., E. Martin, N. Serriari, I. Péguillet, V. Premel, D. Louis, M. Milder, L. Le Bourhis, C. Soudais, E. Treiner, and O. Lantz. 2011. Human MAIT cells are xenobiotic-resistant, tissue-targeted, CD161hi IL-17-secreting T cells. *Blood* 117: 1250–1259.
37. Treiner, E., L. Duban, S. Bahram, M. Radosavljevic, V. Wanner, F. Tilloy, P. Affaticati, S. Gilfillan, and O. Lantz. 2003. Selection of evolutionarily conserved mucosal-associated invariant T cells by MR1. [Published erratum appears in 2003 *Nature* 423: 1018.] *Nature* 422: 164–169.
38. Byrareddy, S. N., N. Sidell, J. Arthos, C. Cicala, C. Zhao, D. M. Little, P. Dunbar, G. X. Yang, K. Pierzchalski, M. A. Kane, et al. 2015. Species-specific differences in the expression and regulation of α4β7 integrin in various nonhuman primates. *J. Immunol.* 194: 5968–5979.

39. Kader, M., X. Wang, M. Piatak, J. Lifson, M. Roederer, R. Veazey, and J. J. Mattapallil. 2009. Alpha4(+)beta7(hi)CD4(+) memory T cells harbor most Th-17 cells and are preferentially infected during acute SIV infection. *Mucosal Immunol.* 2: 439–449.
40. Greathead, L., R. Metcalf, B. Gazzard, F. Gotch, A. Steel, and P. Kelleher. 2014. CD8+/CD161++ mucosal-associated invariant T-cell levels in the colon are restored on long-term antiretroviral therapy and correlate with CD8+ T-cell immune activation. *AIDS* 28: 1690–1692.
41. Voillet, V., M. Buggert, C. K. Slichter, J. D. Berkson, F. Mair, M. M. Addison, Y. Dori, G. Nadolski, M. G. Itkin, R. Gottardo, et al. 2018. Human MAIT cells exit peripheral tissues and recirculate via lymph in steady state conditions. *JCI Insight* 3: 98487.
42. Cicala, C., E. Martinelli, J. P. McNally, D. J. Goode, R. Gopaul, J. Hiatt, K. Jelicic, S. Kottilil, K. Macleod, A. O'Shea, et al. 2009. The integrin alpha4beta7 forms a complex with cell-surface CD4 and defines a T-cell subset that is highly susceptible to infection by HIV-1. *Proc. Natl. Acad. Sci. USA* 106: 20877–20882.
43. Stagg, A. J., M. A. Kamm, and S. C. Knight. 2002. Intestinal dendritic cells increase T cell expression of alpha4beta7 integrin. *Eur. J. Immunol.* 32: 1445–1454.
44. Mora, J. R., M. R. Bono, N. Manjunath, W. Weninger, L. L. Cavanagh, M. Rosemblatt, and U. H. Von Andrian. 2003. Selective imprinting of gut-homing T cells by Peyer's patch dendritic cells. *Nature* 424: 88–93.
45. Svensson, M., B. Johansson-Lindbom, F. Zapata, E. Jaensson, L. M. Austenaa, R. Blomhoff, and W. W. Agace. 2008. Retinoic acid receptor signaling levels and antigen dose regulate gut homing receptor expression on CD8+ T cells. *Mucosal Immunol.* 1: 38–48.
46. Wong, E. B., N. A. Akilimali, P. Govender, Z. A. Sullivan, C. Cosgrove, M. Pillay, D. M. Lewinsohn, W. R. Bishai, B. D. Walker, T. Ndung'u, et al. 2013. Low levels of peripheral CD161++CD8+ mucosal associated invariant T (MAIT) cells are found in HIV and HIV/TB co-infection. [Published erratum appears in 2014 *PLoS One* 9: e95115.] *PLoS One* 8: e83474.
47. Hieshima, K., T. Imai, G. Opdenakker, J. Van Damme, J. Kusuda, H. Tei, Y. Sakaki, K. Takatsuki, R. Miura, O. Yoshie, and H. Nomiyama. 1997. Molecular cloning of a novel human CC chemokine liver and activation-regulated chemokine (LARC) expressed in liver. Chemotactic activity for lymphocytes and gene localization on chromosome 2. *J. Biol. Chem.* 272: 5846–5853.
48. Byrareddy, S. N., J. Arthos, C. Cicala, F. Villinger, K. T. Ortiz, D. Little, N. Sidell, M. A. Kane, J. Yu, J. W. Jones, et al. 2016. Sustained virologic control in SIV+ macaques after antiretroviral and α4β7 antibody therapy. *Science* 354: 197–202.
49. Santangelo, P. J., C. Cicala, S. N. Byrareddy, K. T. Ortiz, D. Little, K. E. Lindsay, S. Gumber, J. J. Hong, K. Jelicic, K. A. Rogers, et al. 2017. Early treatment of SIV+ macaques with an $\alpha_4\beta_7$ mAb alters virus distribution and preserves $CD4^+$ T cells in later stages of infection. *Mucosal Immunol.* 11: 932–946.
50. Sivro, A., A. Schuetz, D. Sheward, V. Joag, S. Yegorov, L. J. Liebenberg, N. Yende-Zuma, A. Stalker, R. S. Mwatelah, P. Selhorst, et al; CAPRISA004 and RV254 study groups. 2018. Integrin $\alpha_4\beta_7$ expression on peripheral blood $CD4^+$ T cells predicts HIV acquisition and disease progression outcomes. *Sci. Transl. Med.* 10: eaam6354.
51. Ericsen, A. J., M. Lauck, M. S. Mohns, S. R. DiNapoli, J. P. Mutschler, J. M. Greene, J. T. Weinfurter, G. Lehrer-Brey, T. M. Prall, S. M. Gieger, et al. 2016. Microbial translocation and inflammation occur in hyperacute immunodeficiency virus infection and compromise host control of virus replication. *PLoS Pathog.* 12: e1006048.
52. Li, H., and C. D. Pauza. 2011. HIV envelope-mediated, CCR5/α4β7-dependent killing of CD4-negative γδ T cells which are lost during progression to AIDS. *Blood* 118: 5824–5831.

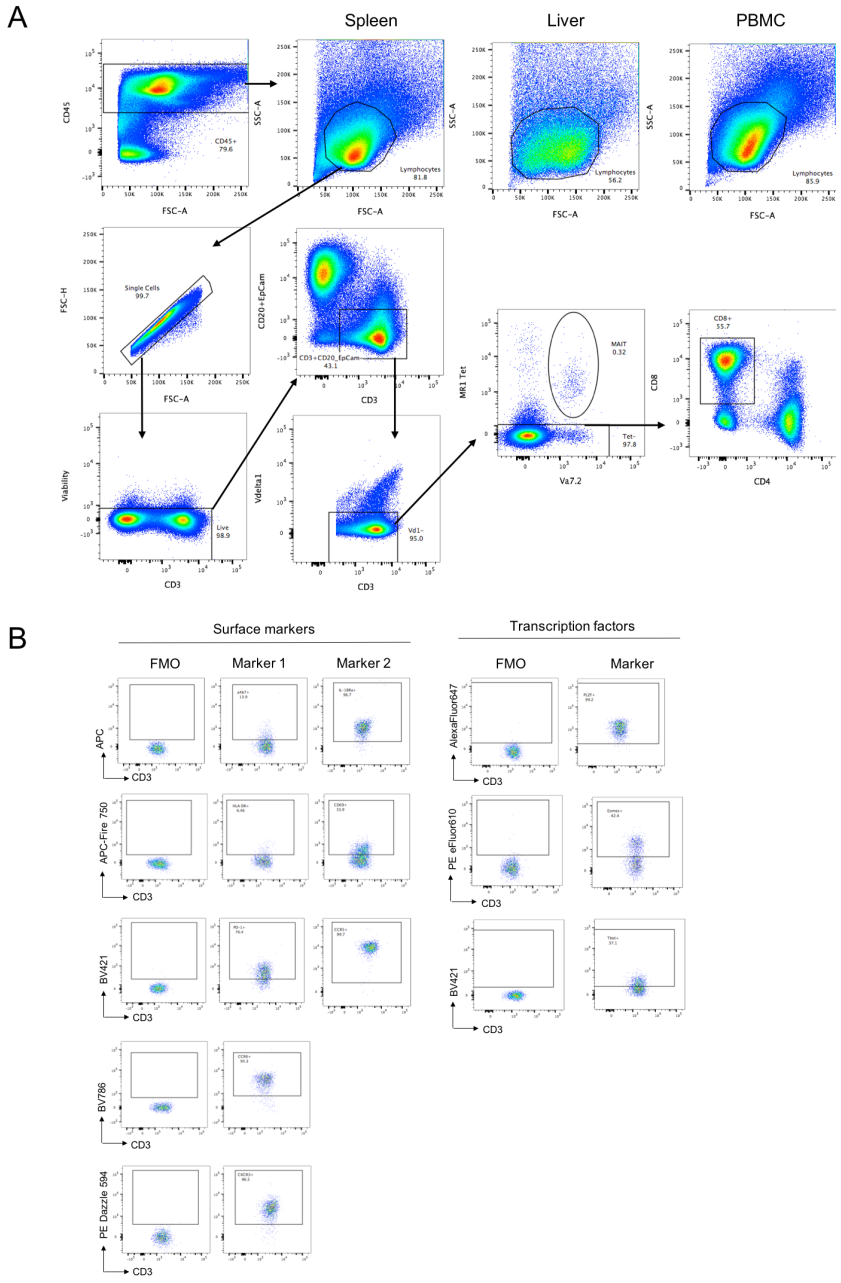

Figure S1. Gating strategy and fluorescent minus one (FMO) controls for MAIT cell identification in PBMC and tissue samples. (A) Single cell suspensions of tissue samples (PBMC, spleen, liver, MLN, ILN and thymus) were analysed based on expression of CD45, followed by gating based on forward scatter (FSC) and side scatter (SSC). Representative scatter of CD45+ cells in spleen, liver and PBMC samples for one animal is shown. Singlets were then identified by FSC-area (FSC-A) versus FSC-height (FSC-H), followed by gating based on viability dye staining. T cells were identified based on the CD3+CD20/EpCam- population, followed by exclusion of Vδ1+ γδ T cells. MAIT cells were then identified as in the rest of the study, based on MR1 tetramer and Vα7.2 co-expression. Conventional CD8+ T cells were identified within the tetramer-negative population as a control. All plots shown are derived from a spleen sample unless otherwise indicated. (B) After gating on CD3+MR1 tetramer+Vα7.2+ MAIT cells, FMO controls for each fluorescence channel and representative staining of antibodies against phenotypic and transcriptional proteins used in flow cytometry panels are displayed.

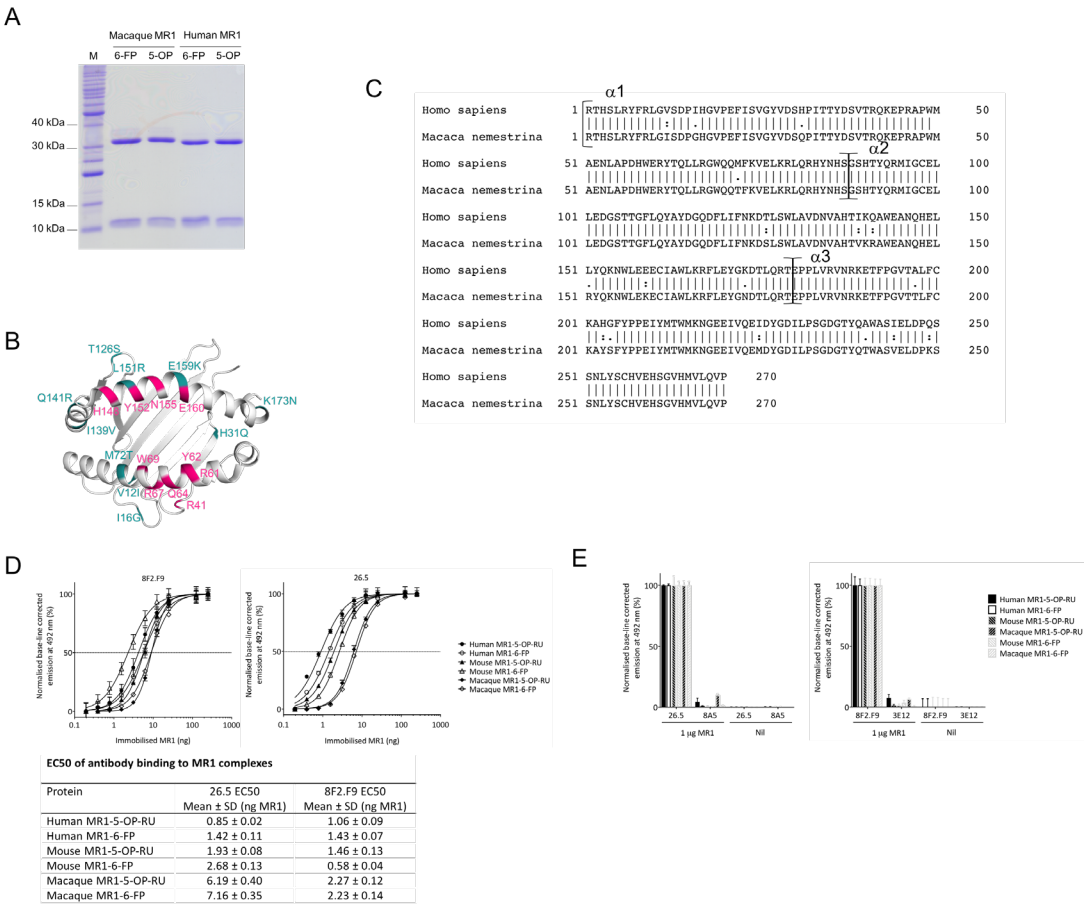

EC50 of antibody binding to MR1 complexes

Protein	26.5 EC50 Mean ± SD (ng MR1)	8F2.F9 EC50 Mean ± SD (ng MR1)
Human MR1-5-OP-RU	0.85 ± 0.02	1.06 ± 0.09
Human MR1-6-FP	1.42 ± 0.11	1.43 ± 0.07
Mouse MR1-5-OP-RU	1.93 ± 0.08	1.46 ± 0.13
Mouse MR1-6-FP	2.68 ± 0.13	0.58 ± 0.04
Macaque MR1-5-OP-RU	6.19 ± 0.40	2.27 ± 0.12
Macaque MR1-6-FP	7.16 ± 0.35	2.23 ± 0.14

Figure S2. Generation and biochemical validation of the *Macaca nemestrina* MR1 monomer. (A) 15 % SDS-PAGE under non-reducing conditions of 1.5 µg purified biotinylated macaque and human MR1 in complex with B2M and loaded with 5-OP-RU (5-OP) or 6-FP in comparison to a protein ladder (M) with molecular weights indicated as relevant. The molecular weights of MR1 and B2M are: macaque MR1: 31,842 Da; macaque B2M: 11,774; human MR1: 31,775 Da; human B2M: 11,862 Da. (B) Cartoon model (generated with the software The PyMOL Molecular Graphics System, Version 2.0 Schrödinger, LLC.) of the MR1 Ag-binding cleft based on the protein data bank (PDB) deposited crystal structure featuring human A-F7 MAIT TCR in complex with human MR1-5-OP-RU (PDB ID: 4NQC[2]). Residues that differ between human and macaque MR1 are highlighted and labelled in teal as follows: human amino acid residues – residue number – macaque amino acid residue. MR1 residues that are contacted in hydrogen bonds (there are no salt bridges) based on analysis using the PDBsum database (ref: PMID: 9433130) of all available crystal structures of human MAIT TCRs complexed with human MR1-5-OP-RU (PDB IDs: 4NQC[2] ; PDB IDs: 4PJ7, 4PJ8, 4PJ9, 4PJA, 4PJB, 4PJC, 4PJD)[54] are highlighted in magenta. All of the human MR1 residues contacted by TCRs in hydrogen bonds are conserved between human and macaque MR1. (C) Sequence alignment of human and *M. nemestrina* soluble MR1, as used as part of this study, indicating the α1, α2 and α3 domains. (D) Assessment of the fold of biotinylated 5-OP-RU and 6-FP loaded macaque MR1 in comparison to human and mouse MR1 in ELISA with 26.5 and 8F2.F9 antibodies showing normalised, base-line corrected dose response curves of triplicate samples with error bars indicating standard deviation. EC50 values, as summarised in a table were determined based on non-linear curve fits shown in the charts. (E) Isotype controls of the assessment of the fold of biotinylated 5-OP-RU and 6-FP loaded macaque MR1 in comparison to human and mouse MR1 in ELISA with 26.5 and 8F2.F9 antibodies shown above.

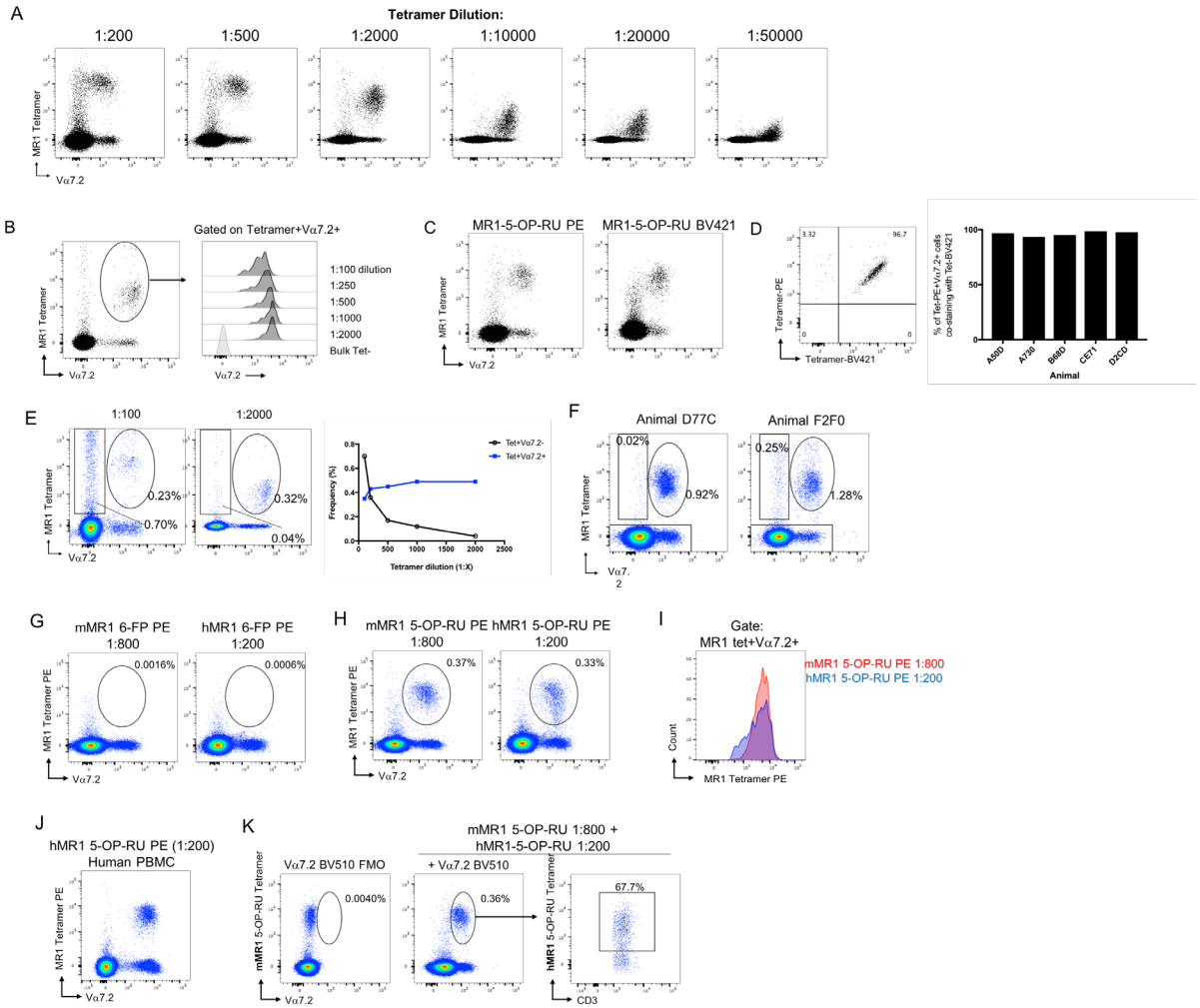

Figure S3. Macaque and human MR1 tetramer staining. (A) Representative staining of macaque PBMC with dilutions of macaque MR1 5-OP-RU tetramer (1:200 to 1:50000). (B) Comparison of Vα7.2 staining intensity on Tetramer+Vα7.2+ cells at decreasing tetramer concentrations compared to MR1 tetramer- cells. Tetramer was added 5 minutes prior to anti-Vα7.2 staining. (C) Identification of tetramer+ Vα7.2+ T cells using MR1-5-OP-RU tetramer conjugated to streptavidin with PE or BV421. (D) Quantification of MR1-5-OP-RU tetramer-PE+Vα7.2+ cells that co-stain with MR1-5-OP-RU tetramer-BV421 in 5 naïve macaques. (E) Quantification of MR1 tetramer+Vα7.2- and MR1 tetramer+Vα7.2+ populations over a tetramer dilution range from 1:100 to 1:2,000. Results are representative of 2 biological and 3 technical replicates. (F) Plots are representative of the variability of MR1 tetramer+Vα7.2- T cell frequencies between among naïve animals at 1:800 tetramer dilution. (G) Staining of fresh PTM PBMC with macaque MR1 (mMR1)-6FP or human MR1 (hMR1)-6FP tetramer (at a dilution of 1:800 or 1:200, respectively) with anti-Vα7.2. (H) Staining of fresh PTM PBMC with mMR1-5-OP-RU or hMR1-5-OP-RU tetramer (at a dilution of 1:800 or 1:200, respectively) in combination with anti-Vα7.2. (I) Histogram of MR1 tetramer staining within the tetramer+Vα7.2+ gates from part B (red, mMR1-5-OP-RU tetramer; blue, hMR1-5-OP-RU tetramer). (J) Staining of human PBMC with 1:200 dilution of hMR1-5-OP-RU tetramer in combination with anti-Vα7.2. (K) Fresh PTM PBMC were co-stained with mMR1-5-OP-RU PE, hMR1-5-OP-RU BV421, and anti-Vα7.2 BV510. Using a Vα7.2 BV510 FMO as a control, mMR1 tetramer+Vα7.2+ cells were identified and subsequently assessed for binding of the hMR1 tetramer. Plots shown in panels A, B, C and E are all derived from the same animal. Results are representative of staining patterns in 3 naïve macaques.

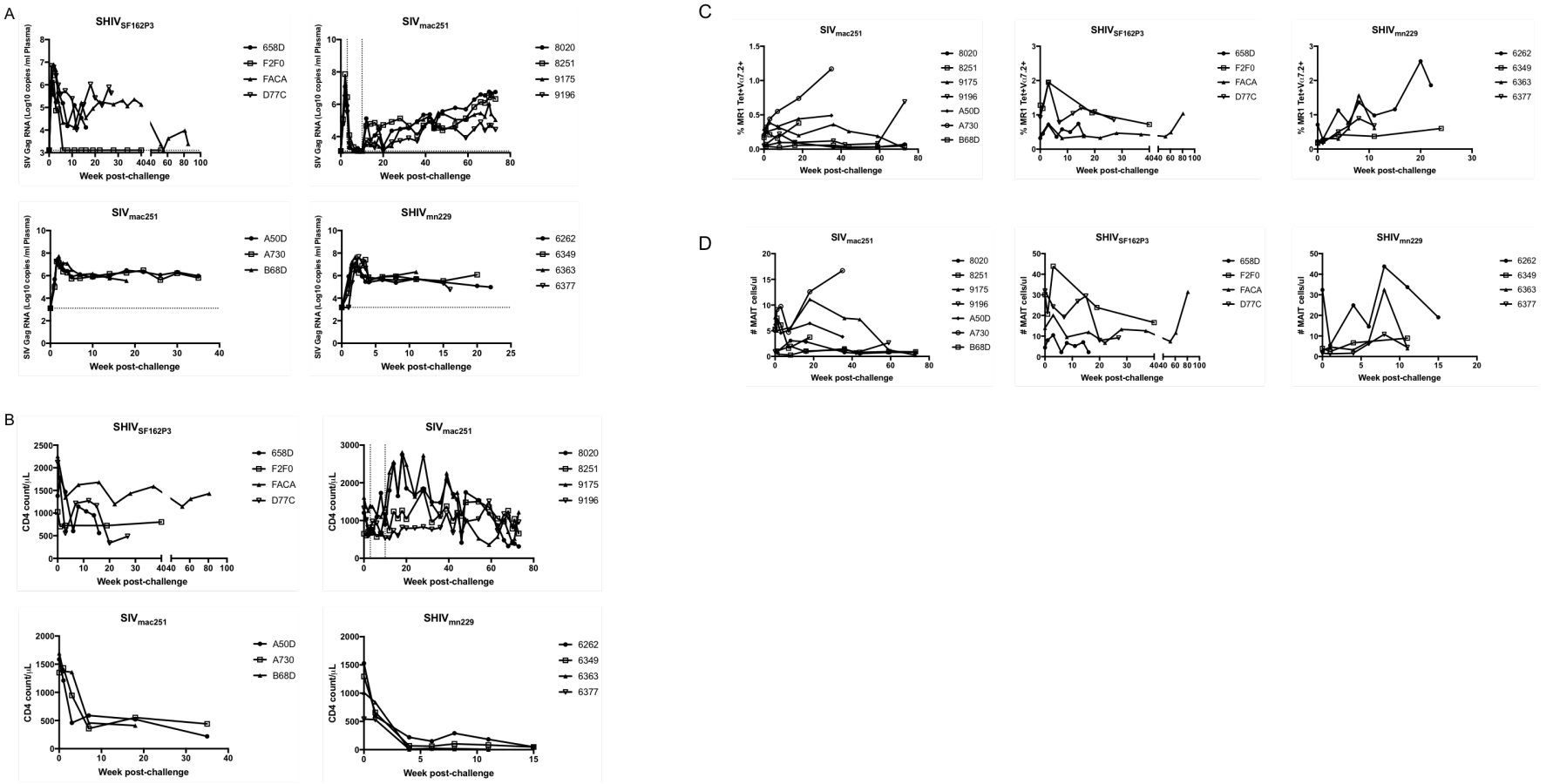

Figure S4. Disease progression and MAIT cell counts of SIV/SHIV infected animals. (A) Viral load (copies RNA/mL of plasma) at each sampling timepoint for animals infected with SIV_{mac251}, $SHIV_{mn229}$ and $SHIV_{SF162P3}$. (B) CD4 counts (per microliter blood) over time for SHIV/SIV infected animals. In some cases, CD4 counts are only available for timepoints selected for analysis in this study. (C) MAIT cell frequency expressed as a percentage of CD3+ T cells or (D) as absolute cell counts per microliter of blood following SIV/SHIV challenge.